KWR 2015.008 | January 2015

# Granular iron(hydr)oxide for phosphate removal from water

Production and market analysis

KWR Watercycle Research Institute

# Granular iron(hydr)oxide for phosphate removal from water

## Production and market analysis

KWR 2015.008 | January 2015

**Project number**
400518

**Project managers**
Marthe de Graaff, Luc Palmen

**Client**
TKI Watertechnologie

**Quality Assurance**
Frank Oesterholt

**Authors**
KWR: Roberta Hofman-Caris, Wolter Siegers, Jan Hofman en RU: Joey Elings, Olaf van der Kolk, Aalke de Jong.

**Sent to**
Reststoffenunie, TKI Watertechnologie

**Year of publishing**
2015

**More information**
Roberta Hofman-Caris
T +31-30-6069673
E roberta.hofman-caris@kwrwater.nl

PO Box 1072
3430 BB Nieuwegein
The Netherlands

T +31 (0)30 60 69 511
F +31 (0)30 60 61 165
E info@kwrwater.nl
I www.kwrwater.nl

KWR Watercycle Research Institute

# Summary

During drinking water treatment iron is removed from groundwater or is added to surface water as a coagulant, which is subsequently precipitated. This results in large amounts (75.000 t/y) of iron (hydr)oxides residuals, formed at drinking water plants in the Netherlands. It is known that these iron(hydr)oxides have a high affinity for phosphate ions. However, the oxides are obtained as aqueous slurries with a rather low solids content (8-10 %).

This project aimed at producing a dry granular material from the iron rich sludges. In this way the residual sludge can be converted into a profitable product that can be packed and shipped more easily and applied in filters for phosphate adsorption. A certain mechanical strength is required, in order to be able to handle them during shipping, and the pellets also should stay stable in a wet form during application, e.g. in a filter column.

The experimental research has shown that wet iron containing sludge can be converted into a granular iron (hyrdr)oxide that is suitable for phosphate removal from surface water. A recipe for production using carboxy methyl cellulose (CMC) as a binder material gives a granular material that is strong enough to use it as a filter medium.

The phosphate adsorption capacity strongly depends on the origin and composition of the iron sludge. Also storage time before drying is an important factor, which may affect the composition of the material. To create a material with a high adsorption capacity, freshly produced sludge is required. The iron(hydr)oxides should be amorphous and the material requires a high specific surface area. As crystallinity increases the material loses its adsorption capacity.

Column experiments have indicated fast adsorption kinetics, high phosphate adsorption capacity (both at high and low phosphate concentrations and at long and short contact times) and good stability of the pellets, even during longer operation periods. For quality control measurement of the specific surface area (Brunauer-Emmett-Teller surface area $S_{BET}$) is proposed.

The product provides water authorities with an interesting technology for phosphate removal from surface waters and in that way contributes to the realisation of the objectives of the Water Framework Directive.

Market analysis has shown that new profitable markets can be entered with the product. These markets can valorize a water treatment residual into a product that enables a profitable business. Moreover, by having an additional market, the risks for drinking water companies to dispose of their residuals is spread in different market segments and will increase guarantees for drinking water companies for selling their residuals.

It is concluded that further development of a market ready product seems to be within reach. It is therefore recommended to start initiatives to scale-up production and develop the supply chain of granular iron (hydr)oxide.

# Contents

# 1 Introduction

## 1.1 General introduction

During drinking water treatment iron is removed from groundwater or is added to surface water as a coagulant, which is subsequently precipitated. Yearly, in the Netherlands this results in about 75,000 tons of iron (hydr)oxides obtained at full scale drinking water plants. About 50,000 tons of this material is obtained as a diluted slurry (ca. 10 wt%) , 27,000 tons has a higher solids content (ca. 30 wt%). It is known that these iron(hydr)oxides have a high affinity for phosphate ions. Removal of phosphate from wastewater or surface water and binding of phosphate in the soil are important issues, for example in the development of natural areas. The large amounts of iron(hydr)oxides produced by drinking water production plants could be very suitable in this respect. However, the oxides are obtained as aqueous slurries with rather low solids contents. For commercial application as adsorbents in phosphate removal the iron(hydr)oxides will have to be pelletized. Only dry pellets can be shipped and used in filters. Besides, these pellets have to have a certain dry strength, in order to be able to handle them during shipping. Furthermore the pellets also should stay stable in a wet form during application. Finally, the pellet quality should be constant and well defined.

## 1.2 Scope of the project

The scope of this project was to develop and test iron(hydr)oxide pellets with sufficient stability and strength, and of constant quality, that can be applied in large scale phosphate removal from water or phosphate binding in soils.

## 1.3 Instruction for reading

Chapter 2 contains an overview of the literature on pelletization of iron(hydr)oxides and phosphate adsorption on the surface of iron(hydr)oxides.

Chapter 3 shows the results of the characterization of two different iron sludges, and the physical and chemical properties of the iron oxides in comparison with commercially available iron(hydr)oxide pellets for e.g. phosphate adsorption. Besides, the characterization of pellets produced by using bentonite or carboxymethyl cellulose (CMC) is described, and results obtained in batch adsorption experiments are presented.

In chapter 4 an overview of some column experiments with two types of iron oxide pellets is given.

# 2 Literature overview: iron pellets for phosphate adsorption in water

### 2.1.1 Introduction

Phosphate ions have a high affinity for iron oxide surfaces. In literature various examples have been described where iron (hydr)oxides are used for removal of phosphates from water. During drinking water treatment iron is removed from the groundwater, or is added as a coagulant, which is subsequently precipitated. As a result large amounts of iron (hydr)oxides are obtained at full scale drinking water plants. It has been shown that iron (hydr)oxides have a high affinity for materials like phosphate and arsenate. If this material can be pelletized, in order to make it easier to handle, it can be used for phosphate or arsenate removal from water on a commercial scale.

### 2.1.2 Pelletisation of iron(hydr)oxides

*Purpose of pelletization*

Iron containing sludges are relatively difficult to handle, as they contain 70-90% of water. Although the iron(hydr)oxides may be good adsorbents, transport of the wet sludge to a site where it can be applied will be very expensive. Furthermore, it is not sure that all sludges will have the same composition of the iron(hydr)oxides; in fact is even is unlikely that this will be the case. As a result the (adsorption) properties of the material may differ, rendering application of the material complicated. Previous drying of the sludge would solve these problems: the wet sludge now only will have to be transported to the site where it will be processed, and by mixing material of different drinking water production sites constant quality can be assured. However, drying will result in iron(hydr)oxide powder or very brittle particles that will easily turn into powder, which too is very difficult to handle. This problem has been known in mining industry for several decades, and there it was solved by pelletizing the ironoxides before transport. The pellets thus obtained should be a little elastic, in order to prevent them from breaking during transport or application in the steel industry. However, the elasticity should not be too high, as otherwise deformation would occur, resulting in a thick and dense layer of ironoxides, instead of in discrete pellets. In this project experiences from mining industry were taken into account, as the problems encountered are more or less similar.

*Techniques that can be used*

Iron ores consist of a fine powder, that is very difficult to handle. Therefore it is common practice to pelletize the oxides, in order make handling easier. There are several techniques that can be applied, like briquetting, balling, tableting and pelletizing. Pelletization is the unit operation of agglomerating moist particulate materials by tumbling them in horizontal rotating drums or inclined discs [Tugrul et al., 2007]. In general a binder will be applied, in order to improve the strength of the pellets. The main effective ore properties are its specific surface area, porosity, mineralogical composition, and particle size distribution of the material [Abouzeid and Seddik, 1981]. Apart from the binder, the moisture content plays a crucial role. A binder should possess the ability to regulate the motion and distribution of water through the feed and improve the strength of the pellets.

For iron ores two types of pellets are distinguished: green pellets and dried pellets. Green pellets are pellets formed at room temperature, containing moisture. This moisture content is critical, with the optimum at a concentration at which water is collected in every surface pore [Mohamed et al., 2003]. Insufficient moisture causes air inclusions and reduces the capillary forces, which are very important for the strength of the pellets [Qiu et al., 2003]. On the other hand, an excess of moisture would form a coherent film of water, neutralizing the capillary effect. For steel production these pellets are heated up to > 1100 ºC. In the first stages of the heating process water is removed, resulting in "pre-heated" and "dry" pellets. At higher temperatures (1200-1300 ºC) sintering of the iron oxides occurs, due to oxidation of magnetite to hematite and crystal growth and recrystallization. Thus, the pellets become stronger (so called "fired pellets") [Oglonlowo, 1989]. In steel production processes carbon is added, in order to raise the temperature by burning the carbon.

*Bentonite as a binder material*

For decades bentonite has been used as a binder in iron ore pelletization [Abouzeid and Seddik, 1981; Luo et al., 2011]. Bentonite proved to be effective in increasing the pellet strength and in controlling the moisture content. It is used at 0.5-1.5% addition levels (100 and 200 mesh sieve sizes) by weight of iron ore [Sivrikaya and Arol, 2011, 2012]. Increasing the amount of bentonite (from 0.5 to 1.2%) increases the wet-crush strength of the pellets [Sivrikaya and Arol, 2011]. However, increasing the bentonite concentration also retards the ball growth rate in balling processes, as a result of the immobilization of water by bentonite. At a constant bentonite amount the growth rate of the pellets increases with increasing moisture content [Ogblonlowo, 1989]. The differences in behavior between different bentonites are not completely predictable simply from measurements of their water absorption capacity [Kawatra and Ripke, 2003]. Other bentonite properties may also have a strong influence on the binding strength of a given bentonite and on its sensitivity to dissolved ions in the water.

Bentonite is a mixture of layered hydrated aluminosilicate clays, which is primarily composed of smectite class mineral montmorillonite, with the general formula:

$$(Na, Ca)_{0.33}(Al_{1.67}, Mg_{0.33})Si_4O_{10}(OH)_2.nH_2O$$

Its crystalline structure consists of highly stable three-layer aluminosilicate platelets that are loosely held together by electrostatic forces.

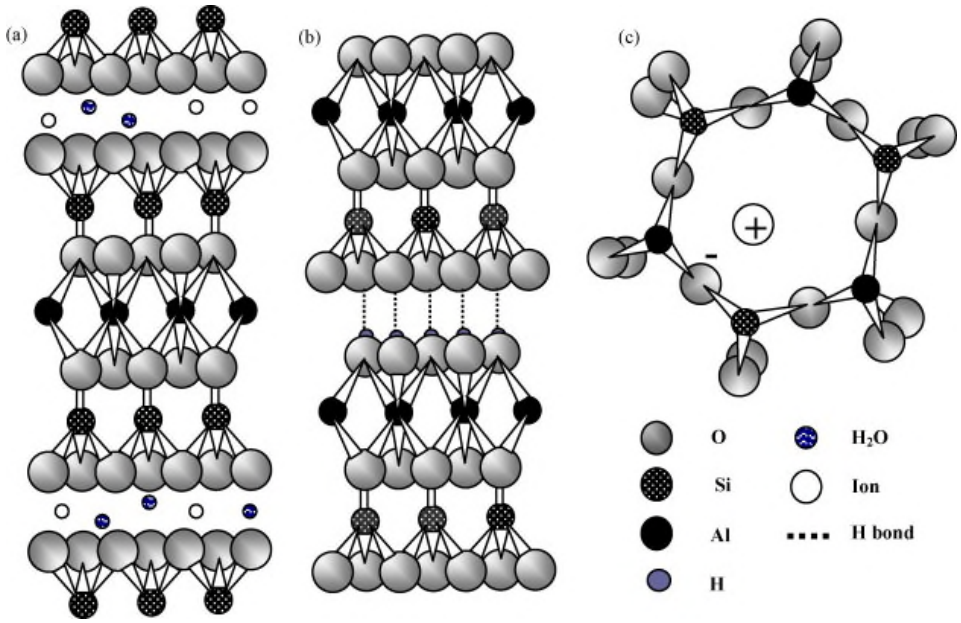


*Figure 1. Chemical structure of (a) bentonite (montmorillonite), (b) kaolinite, and (c) zeolite [Vimonses et al., 2009].*

Bentonite dilates after absorbing water and in water disperses into a colloid. The positive ions in the lattice layer form hydrated ions that are loosely bound with the lattice and can be replaced by other ions in the solution. Ion exchange mainly occurs between the lattice layers and does not cause changes in the lattice skeleton [Shu et al., 2012].

For steel production the main disadvantage of bentonite is that it contains silica and alumina. Some forms of sodium bentonite contain more than 65% $SiO_2$ by weight or 85% $SiO_2$and $AL_2O_3$ [Sivrikaya and Arol, 2012]. The silica may block the porosity of the pellet and does not contribute to the cohesive and adhesive forces maintaining the pellet's integrity. Isomorphic substitution of $Al^{3+}$ by $Mg^{2+}$ within the platelets alters the crystal charge balance, giving the lattice a net negative charge. This results in the adsorption of cations like $Na^+$ and $Ca^{2+}$ to balance the charge. The hydration of these exchangeable interlayer cations allows water to be absorbed between the layers of the crystal, causing it to expand upon wetting. The layers are separated by an exchangeable cation layer. Sodium bentonites are more highly absorbent than calcium bentonites as the divalent calcium ions hold the clay platelets more strongly together than monovalent sodium ions. Apart from the larger swelling index, sodium bentonite also shows better dispersivity in water, and higher plasticity and cohesiveness. This makes it more suitable for pelletising [Fan et al, 2011]. Thus, also a lower bentonite dose can be applied [Fan et al, 2011]. However, initially calcium bentonite appears to absorb water faster than sodium bentonite. This is important for ore pelletization processes [Kawatra and Ripke, 2003]. If $Ca^{2+}$ and $Mg^{2+}$ are present in water, they can displace $K^+$ and $Na^+$, thus increasing the bonding between the bentonite platelets, weakening their expansion and reducing the absorbency of water. Artificial modification of natural bentonite can be carried out using pulping sodium, stacking sodium, extrusion sodium, wheel rolling sodium and microwave sodium treatments [Shu et al., 2012].

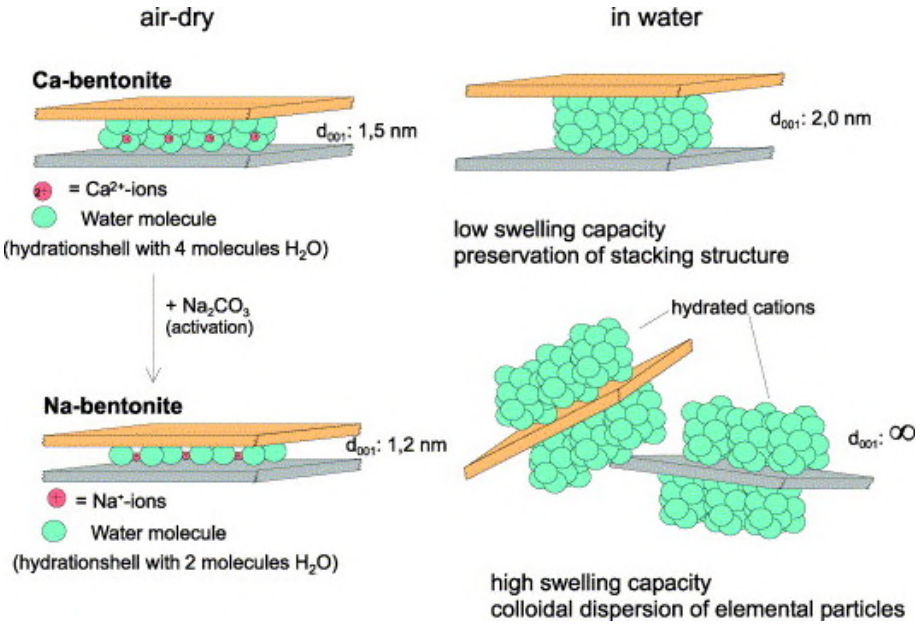


*Figure 2. Effects of Na and Ca ions in bentonite behavior [Koch, 2002].*

Bentonite increases the dry strength of iron ore pellets in two ways. First, it provides a source of colloidal material that decreases inter particle distances, thus increasing van der Waals forces. Secondly, it forms a solid bridge of hardened gel that strengthens particle contact points. When bentonite clay is moistened, it begins expanding and the electrostatic attraction between the individual platelets becomes relaxed, allowing the platelets to slip across each other and spread like a deck of cards pushed across a table. Effective binding occurs when the bentonite platelets slide past one another to form sheet-like or fiber-like structures. This can be realized when compression and shear forces are applied, like in compressive shear mixing [Kawatra and Ripke, 2003]. Milling together the concentrate and bentonite causes them to contact closely, enabling bentonite to fully display its cohesive characteristics, and thus enhancing the strength of the green pellets [Fan et al., 2011].

*Alternative binders*

Especially for steel production, the presence of Si and Al in bentonite is a disadvantage. Therefore, several alternative binder materials have been tested and described in literature. The use of colemanite, a calcium-borate salt with the chemical formula $CaB_3O_4(OH)_3.H_2O$, was described by [Sivrikaya and Arol, 2011 and 2012]. It was combined with other binder materials, both organic binders (like carboxymethyl cellulose (CMC), and corn starch) and inorganic materials (such as NaOH, $Na_2CO_3$, CaOH, $CaCl_2$, fly ash etc.).

According to [Qiu et al, 2003], the ideal organic binder for iron ore pellets should possess the following characteristics:

- Hydrophilic groups enforcing wettability of the ore particle surface
- Polar groups which can react with the iron ions (COO, OH, $CONH_2$, $NH_2$, $NO_2$, NH, $NR_3$, $PO_3H$, $SO_3H$, $OSO_3H$, SH etc.). Groups containing phosphorous and sulphur are detrimental for the steel quality.
- Strong and heat resistant organic chain skeleton, preferentially containing unsaturated groups and aromatic ring structures.

Organic binders with a relatively low molecular weight will show a relatively weak interaction among adjacent chains. This improves with increasing molecular weight. The higher the molecular weight of a binder, the greater its mechanical strength and thermal stability will be. However, the viscosity of a polymer solution will increase with increasing molecular weight, reducing the wettability of the iron oxides. The presence of double, and triple bonds and of aromatic or heterocyclic rings has a positive effect on the binder properties of material. If the hydrophilic group is an electron-withdrawing group (e.g. $SO_3H$, $NO_2$ or COOH), it will reduce the affinity of polar groups. If the hydrophilic group is an electron-donating group (like $NH_2$, OH, SH etc.) it will enforce the affinity of polar groups. Besides, the relative position of the hydrophilic group to the polar group also affects the efficiency of the binder material. It was shown that a COO polar group in combination with OH as a hydrophilic group is very suitable.

Very often polycarbohydrates are used as binder materials. Examples are modified starch and modified cellulose, like carboxymethyl cellulose (CMC). The latter is commercially available, e.g. under the brand name “Peridur”. For application in phosphate removal from water, such organic binders might be less suitable, as they may tend to absorb water, resulting in swelling and ultimately even disintegration of the pellets. However, so far CMC has not been used for this purpose, and there is no information available on this topic yet.

Dissolved natural organic matter (DOM) can influence the behavior of metal ions to a large extend. Dissolved organic matter is a complex mixture of many molecules (mainly humic and fulvic acids), usually operationally defined as the organic matter that can pass a 0.45 µm filter. It can affect the solubility of metals, as complexation with DOM can increase the concentration of dissolved metals by more than two orders of magnitude. pH plays an important role in this phenomenon. Two types of models, Model VI and nonideal consistent competitive adsorption (NICA)-Donnan were applied by [Weng et al., 2002] and [Milne et al., 2003]. The NICA-Donnan model can describe the binding of metal ions to fulvic acids (FA) or humic acids) (HA) over a wide range of conditions, and generic model parameters are given for 23 metal ions, including Fe(II) and Fe(III).

### 2.1.3 Phosphate adsorption

*Phosphate adsorption on iron(hydr)oxides*
It is well known that iron oxides can effectively adsorb phosphates. This depends on one hand on the anions’ complexing capacity, allowing binding to surface groups by ligand exchange reactions, and on the other hand on electrostatic interactions with the charged (hydr)oxide surfaces [Zach-Maor et al., 2011]. Phosphate can adsorb on iron oxides to form a variety of surface species, including mononuclear monodentate, mononuclear bidentate, and binuclear bidentate. The equilibrium between phosphate ions in solution and solid surfaces depends on the concentration of phosphate ions in solution, the pH of the suspension, ionic strength and temperature. However, in most cases iron oxides present slow adsorption kinetics owing to diffusion resistance of the interior of the oxide. Following diffusion, some of the outer iron oxide binding sites become available for further phosphate uptake.

Orthophosphate ions have a high affinity for oxide surfaces. According to IR analysis, the dominating surface complexes are three species that are monodentately coordinated to the iron (III) ions at the surfaces, and mainly differ in their degree of protonation, namely:

- $Me\text{-}O\text{-}PO_3H_2$
- $Me\text{-}OPO_3H^+$
- $Me\text{-}OPO_3^{2-}$

The surface speciation strongly depends on pH, and inner-sphere surface complexes were shown to be formed [Persson et al., 1996]. The phosphate surface species on goethite show all characteristics of true surface complexes, like a reversible protonation as a function of pH, and IR spectral properties in agreement with complex formation. On hematite, however, the phosphate ions display a very different behavior, resulting in the formation of a three-dimensional surface precipitate.

[Mao et al., 2012] found that an increase in pH, age of hydrous ferric oxides (HFO) and concentration of competing anions negatively affects the phosphate adsorption capacity. Two models, a semi-empirical diffuse layer model (DLM) and a molecular model (CD-MUSIC), were used to describe the phosphate adsorption. For both models the authors give a list of key reactions and associated constants. According to [Arai and Sparks, 2001], phosphate adsorption decreases with increasing pH 3.5 – 9.5, but is insensitive to changes in ionic strength at pH 4 – 7.5. At pH > 7.5 it slightly increases with increasing ionic strength from 0.01 to 0.8. These authors used ATR-FTIR to demonstrate that inner-sphere complexes are nonprotonated, bidentate binuclear species ($\equiv Fe_2PO_4$) at pH ≥ 7.5, and could be associated with $Na^+$ ions at P loading levels of 0.38 µmol/$m^2$. At pH 4-6 protonated inner-sphere complexes are proposed at loading levels between 0.38 and 2.69 µmol/$m^2$ .

[Zhou et al., 2012] describe the use of hydrated ferric oxide nanoparticles, immobilized onto macroporous activated carbon fibers. The phosphate adsorption in this case was fitted by Langmuir isotherms. It was found that the adsorption capacity of these materials was relatively low, probably as a result of the lower iron (hydr)oxide surface available for anion adsorption and/or the uneven distribution of iron in the GAC particles due to poor iron penetration. [Zach-Maor et al., 2011] studied phosphate adsorption by a homogeneous porous layer of nano-sized magnetite particles immobilized onto granular activated carbon. They found that phosphate bonding took place predominantly through bidentate surface complexes.

Iron oxides can also be combined with polymer materials, like anion exchange resins [Pan et al., 2009]. [Cong and Yu, 2011] combined macroporous $Fe_2O_3$ with organic colloidal crystals like poly(styrene-methyl methacrylate-acrylic acid), and [Sadakane et al., 2010] used macroporous perovskite-type lanthanum-iron-oxide ($LaFeO_3$) with polymethyl methacrylate and ethyleneglycol.

According to [Zach-Maor et al., 2011], iron oxides containing phosphates can be regenerated by treatment with an alkaline eluent such as NaOH. It is worthwhile investigating whether this regeneration process can be applied to our pellets.

*Effect of Natural Organic Matter (NOM) on phosphate adsorption*

[Weng et al., 2008] studied the interactions between humic acid (HA) or fulvic acid (FA) with phosphate ions at the surface of goethite. Humics (both FA and HA) are mixtures of complex molecules, showing a large degree of chemical heterogeneity. Clear differences were found between HA and FA in their interactions with phosphate at the surface. Although HA is strongly bound to goethite, it does not strongly affect the phosphate binding. FA, on the contrary, is less strongly bound but has a very large effect on the phosphate adsorption and vice versa. In both cases electrostatic forces are involved. The FA (with a diameter of about 1-2 nm) is adsorbed closer to the oxide surface, resulting in a stronger electrostatic interaction between adsorbed FA and phosphate ions. This is explained by the larger physical size of HA, as a result of which HA has to be positioned in the diffuse double layer beyond the compact part of the electric double layer. Phosphate ions have the smallest size. It was found that on average 90 phosphate ions can be adsorbed per 100 $nm^2$ (in the pH range studied), which is

about 14 mg/m$^2$, whereas 25-50 mg/m$^2$ HA and 10-35 mg/m$^2$ FA (about 15-30 molecules per 100 nm$^2$) could be adsorbed. Thus, also the higher concentration of FA at the surface will probably affect the phosphate adsorption.

*Dutch phosphate adsorption studies*
In the Netherlands several studies have been carried out on the adsorption of phosphate by means of iron oxides [Stowa, 1994; Dammann and Benzinger, 1995; Voortman and van den Heuvel, 2002; Koopmans et al., 2010; Joosten, 2004]. In most cases iron (hydr)oxides were found to be very effective for phosphate removal. [Joosten, 2004] reported an adsorption capacity of phosphate on surface water sludges of 0.04-0.08 mol per mol iron, which is in accordance with the data given by Stowa [Stowa, 1994] of 0.04-0.11 mol/mol (0.02-0.06 g P / g Fe) in the pH range 7-8. At lower pH values the adsorption increases. For ground water 0.09 – 0.15 mol phosphate per mol iron was found. According to [Koopmans et al., 2010], iron oxides from water treatment plants can adsorb more phosphate than e.g. goethite, which among others has a much lower specific surface area [Nooijen, 1984; Stowa, 1994]. However, upon aging the ferrihydrite may recrystallize, resulting in a higher goethite content. It was also found that adsorption of phosphate onto the iron(hydr)oxides takes time. [Voortman and van den Heuvel, 2002] concluded that *iron*(hydr)oxides from water treatment plants can be pelletized, but that addition of bentonite is necessary, as otherwise organic matter present would destroy the coherence of the pellets. In their study it was found that the iron(hydr)oxides contained a relatively large arsenic concentration, which may render it difficult to apply. This problem also was mentioned in the Stowa report [Stowa, 1994]. It may be a disadvantage, especially when acidified precipitate is used in order to increase its adsorption capacity. At lower pH, the arsenic present in the precipitate will be dissolved more easily.

### 2.1.4 Patents on iron oxide pelletisation
A limited patent search was carried out in the field of iron (hydr)oxide pelletization.

- In WO 02/26630 A1 an aqueous dispersion of iron hydroxide is mixed with polymer dispersion, and the mixture is dried until dry particles are obtained.
- In WO 02/26631 an aqueous dispersion of iron (hydr)oxide is mixed with Mg and/or Al (hydr)oxides, and dried.
- This is comparable to the procedure described in EP 1 344 564 A2, where the iron (hydr)oxide is mixed with other materials like Al, Mg, Mn or Ti (hydr)oxide, activated carbon or zeolites and Cu-, Zn- or Ag-containing compounds. The aqueous mixture is dried and grinded or granulated.
- In EP 1 328 476 B1 first an aqueous dispersion of $\alpha$-FeOOH is made by treating iron salt solutions with an excess of NaOH. After subsequent oxidation the water and dissolved compounds are removed.
- This procedure resembles the procedure described in EP 1 582 505 B1, where Fe(III) salts are reacted with a base at pH 6-8.
- In EP 1 328 478 B1 aqueous $\alpha$-FeOOH is combined with Al(OH)3 or $Mg(OH)_2$ and dried.

None of these procedures is similar to the procedures applied in the research described in this report.

### 2.1.5 Relevance for this research
The relevance of the literature study in the previous paragraphs for this study can be summarized as follows:

- Pelletization of iron(hydr)oxides can be carried out in different ways. The easiest way is by simply drying, sieving and mixing of the material.
- In order to obtain stable iron(hydr)oxide pellets a binder should be applied.
- Bentonite is a commonly used binder material for iron(hydr)oxide pellets. Bentonite types with special modifications for this purpose are commercially available.
- CMC is an alternative organic binder that is commercially used for this purpose.
- Iron oxides can be very effective for phosphate removal, although the adsorption capacity seems to depend on the exact composition of the material.

# 3 Preparation and characterisation of granular iron(hydr)oxide

## 3.1 Materials and Methods

### 3.1.1 Preparation of granular iron(hydr)oxide

Three different samples of iron(hydr)oxide sludge from drinking water companies were used in this project:

- Spannenburg: obtained from ground water. Solids content 8 wt%
- Kralingen: obtained from surface water. Solids content 32 wt%
- Witharen: obtained from ground water. Solids content 11%. This sample was only used in a column adsorption experiment (see Chapter 5).

Three different strategies for pelletization of this material were followed:

1. Iron(hydr)oxide samples of Spannenburg and Kralingen were dried at 105 °C, and subsequently ground and sieved, until a size range of 0.6-1.4 mm was obtained.
2. The aqueous sludge (Spannenburg and Kralingen) containing iron(hydr)oxide was mixed with 1 or 2 wt% (based on solids) bentonite (applied as an aqueous sludge), for which two types were used: Cebogel Bondex and Cebogel IPR-012 (both sodium bentonites specially modified for binding of pellets), using a magnetic stirrer. Subsequently the samples were dried at 105 °C, and ground and sieved, until a size range of 0.6-1.4 mm was obtained.
3. The aqueous Spannenburg sludge containing iron(hydr)oxide was mixed with 1 or 2 wt% (based on solids) of carboxymethyl cellulose (CMC; CAS 9004-32-4 Type Gabrosa P300D Batch/ID 2%Brf.9500mPa.s), specially designed for binding of iron pellets in mining applications. The CMC was added as a powder under high shear in a blender. Subsequently the sample was dried at 105 °C, and ground and sieved, until a size range of 0.6-1.4 mm was obtained.

These pellets were characterized and used for phosphate adsorption experiments.

### 3.1.2 Characterisation of iron(hydr)oxide

Both the Spannenburg and Kralingen materials were characterized at Delft Solid Solutions[1]. Later limited characterization of the Witharen sample was carried out by the same laboratory.

Both materials (Spannenburg and Kralingen) were compared with FerroSorp®. This is a commercially available adsorbent based on ferric hydroxide, which is produced from the iron(hydr)oxide containing sludges of drinking water purification plants in Germany.

*$N_2$ adsorption*

Prior to the $N_2$ adsorption measurements, the samples were degassed in vacuum at 90°C for 16 h. The dry sample weight obtained after the pre-treatment has been used in the various calculations. Adsorption and desorption isotherms with $N_2$ as adsorptive were then recorded at 77 K on a Micromeritics TriStar 3000.

[1] Delft Solids Solutions B.V., PO Box 180, 2290 AD Wateringen, The Netherland

In $N_2$ physical gas adsorption, the sample cell holding the degasified sample is evacuated and cooled to liquid nitrogen temperature (77 K). Portions of nitrogen are dosed into the sample cell and will be partly adsorbed on the surface, eventually getting into equilibrium with the gas phase. In this way adsorption and desorption points are recorded at different pressures and the ad- and desorption isotherm can be constructed.

Adsorbed nitrogen will first form a quasi-monolayer on the sample surface while further increase in pressure results in the formation of multilayers. In the region where monolayer and multilayers are formed, the specific surface area ($S_{BET}$) is determined according to the BET (Brunauer, Emmet and Teller) theory. This model is applicable to non-porous and meso and macro porous materials and adsorption points in the relative pressure range between 0.05 and 0.25 are typically used. In case meso pores are present in the sample under investigation, $N_2$ will condense in these pores at higher relative pressures. This information can be used to derive a meso pore size distribution, typically by means of the so called BJH (Barrett Joyner and Halenda) pore size model. Besides, the empirical t-plot methodology can be used to discriminate between contributions from micro pores and remaining porosity (i.e. meso porosity, macro porosity and external surface area contributions).

*Mercury intrusion porosimetry*
Mercury intrusion porosimetry (MIP) measurements are performed on a variety of samples to determine the pore volume, porosity, and the pore size distribution. This technique is based on the principle that mercury is a non-wetting liquid and requires a force to penetrate voids.

In a typical analysis, pressures from approximately 0.01 kPa to 200 MPa are applied and application of the Washburn equation converts the pressure to pore diameter ($d_{pore}$) according to the following relationship:

$$d_{pore} = \frac{-4\gamma cos\theta}{p} \qquad (1)$$

A value of 140° is used for the contact angle ($\theta$), as this has proven to be a realistic value for most oxidic materials, while the surface tension of mercury ($\gamma$) amounts to 0.48 N/m. Measurement of the volume displacement by the solid sample also enables to assess its density. In a typical experiment, the contributions from pores covering the range of approx. 800 micrometers down to 5 nanometers can be assessed quantitatively.

The pore volume was only measured for the Ferrosorp sample. This MIP experiment has been carried out on a Micromeritics Autopore 9505 porosimeter in the pressure range from vacuum up to 220 MPa. Prior to the measurement, the sample has been pre-treated in an oven at 90°C for 16 h. The dried sample was then transferred and weighed in the sample holder. Approximately 0.35 grams of dry sample has been used in the analysis and the dry sample weight has been used in the various calculations.

*X-Ray Diffraction*
The atomic and molecular structure can be attained by X-ray diffraction investigations. Crystalline atoms cause diffraction of an X-ray beam into specific directions, leading to typical reflections at certain characteristic positions in the XRD profile. In that way, the presence of crystalline matter can be identified; amorphous matter typically results in very broad, ill-defined reflections.

The X-ray powder diffraction (XRPD) patterns were recorded in a Bragg-Brentano geometry in a Bruker D5005 diffractometer equipped with Huber incident-beam monochromator and Braun PSD detector. Data collection was carried out at room temperature using

monochromatic Cu radiation (K$\alpha$1 $\lambda$ = 0.154056 nm) in the 2$\theta$ region between 15° and 95°, step size 0.035 degrees 2$\theta$.

The sample, of about 30 milligrams, was deposited on a Si <510> wafer and was rotated during measurement. Data evaluation was done with the Bruker program EVA.

*X-Ray Fluoresence*
The chemical composition of the various samples has been investigated by means of the multi-element technique X-Ray Fluorescence (XRF). X-ray fluorescence is a non-destructive analysis for the qualitative and semi-quantitative determination of elements with an atomic weight ≥ carbon (Z ≥ 6). X-ray fluorescence is based on the principle that an atom is irradiated by high-energetic radiation and releases an electron from a valence shell of the atom. A higher placed electron takes the vacant place and transmits element-characteristic radiation. The intensity of this radiation is a guideline for the concentration of the concerned element.

Semi-quantitative determination of the multi-element composition of the three samples has been attained in a PANalytical Axios-Max XRF spectrometer. Prior to the analysis, the three samples were milled followed by drying in an oven at 90°C. Subsequently, a suitable pellet has been generated by means of pressing about 1.5 g of the powdered sample with boric acid without binder; this assists in homogenization of the sample and it minimizes matrix effects.

*Crushing strength*
The robotic compression tester (RCT) is an instrument for measuring the strength of particles and granules with limited supervision.

The robotic compression tester measures the maximum crushing force of individual particles or granules. The crushing force of particles with sizes ranging from 500 μm to 5000 μm can be measured. About 40 up to 100 particles are placed on a 2 cm thick smooth finely polished stainless steel plate and the coordinates of each particle and size are determined by a CCD camera. Consecutively all particles at the known coordinates are crushed and the required force is measured with a quartz force transducer. The transducer is a device that uses the piezoelectric effect to measure pressure, acceleration, strain or force by converting them to an electrical charge. The sensitive transducer is suitable for measuring quasi-static and dynamic tensile and compressive forces ranging from a few mN to 100 N.

The principal result of the compression test is an average maximum crushing force and the particle size distribution. Compressive strength of particles and agglomerates is often proportional with the particle diameter, the relationship is generally in the form:

$$L = k\,D\,n \qquad (2)$$

where $L$ is the crushing force, $D$ is the particle diameter, $k$ and $n$ are constants depending on the material.

### 3.1.3 Phosphate adsorption

Phosphate adsorption experiments were carried out using a phosphate solution with a concentration of 100 mg $PO_4$/L. For these experiments the water should be free of calcium ions as these may precipitate with the phosphates. Analyses were carried out using Hach Lange phosphate test kits. Solids concentrations were varied from 100 to 3200 mg/L. The fraction with a size range of 0.6 to 1.4 mm was used in adsorption experiments.

### 3.1.4 Adsorption isotherm studies

Adsorption isotherm studies were performed using Schott glass bottles of 1 L. Different masses of adsorption material (100 – 3.200 mg) were added to 6 bottles, then 1 L of Ca-free drinking water (Tull en 't Waal) with 100 mg $PO_4$ /L was added. A blank was prepared by adding the water to a bottle without adsorption material. The solution was stirred gently, to prevent breakage of the pellets, for two weeks in a dark oven at 105 ºC till equilibrium was reached. After filtration over 0,45 µm filters, the phosphate concentration was measured in the water.

## 3.2 Results and discussion

### 3.2.1 Starting Material

Two different samples were used: iron from the groundwater production site in Spannenburg, and iron from the coagulation process at production site Kralingen. The Spannenburg material only contained 8% solids, whereas the Kralingen sample contained 32% solids but was contaminated with little stones and twigs. Pictures of these samples are shown in Figure 3.

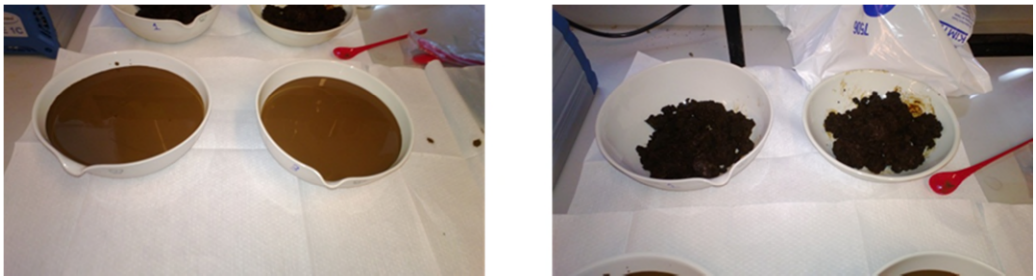

*Figure 3. Iron sludge from Spannenburg (left) and Kralingen (right).*

Both samples were dried at 105 ºC or at 40 ºC. Subsequently, they were ground and sieved, until a size range of 0.6-1.4 mm was obtained. These particles were analysed and compared to commercially available iron pellets (FerroSorp®), with a size range of 0.5-2 mm. The resulting materials are shown in Figure 4.

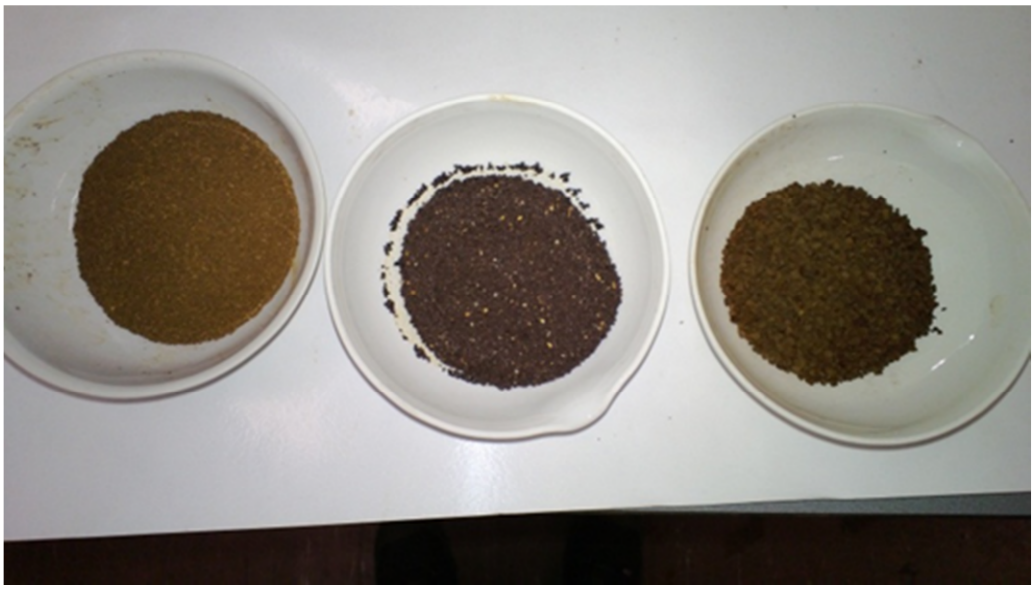

*Figure 4. Iron(hydr)oxide pellets from Spannenburg (left), Kralingen (middle) and commercially available Ferrosorp (right)*

These particles were characterized as described in section 3.1.2 (Appendix I)

Nitrogen adsorption and desorption isotherms were obtained. In the relative pressure[2] range of approximately 0.05-0.25 different volumes of nitrogen were adsorbed, indicating a different surface area available for adsorption, since in this pressure range a monolayer is observed. Based on these results the BET surface area was calculated, as shown in Table 1.

TABLE 1. TEXTURAL PROPERTIES OF THE FERROSORP, SPANNENBURG (RAW MATERIAL) AND KRALINGEN (RAW MATERIAL) SAMPLES, AS DERIVED FROM THE NITROGEN ADSORPTION EXPERIMENTS.

| Sample | $S_{BET}$ ($m^2/g$) | $V_{pore}$ ($cm^2/g$) |
|---|---|---|
| Ferrosorp | 276 | 0.640 |
| Spannenburg (raw material) | 230 | -- |
| Kralingen (raw material) | 117 | -- |

In Figure 5, Figure 6 and Figure 7 the XRD patterns of the three samples are shown. From this comparison it becomes clear that distinct similarities as well as differences are found among the three samples. The Ferrosorp reference sample (Figure 5) presents mostly broad amorphous contributions with one strong reflection at about $2\theta = 35°$. This can be assigned to the presence of a calcite ($CaCO_3$) phase. The same characteristic reflection can also be found in both samples Kralingen and Spannenburg, indicating that here too calcite is present. The Spannenburg sample (Figure 6) also presents a mostly amorphous structure with one contribution of calcite, and thus appears to have a similar structure as the Ferrosorp sample. Compared to the Ferrosorp sample, however, this calcite contribution tends to have a much lower intensity, and thus it can be concluded that a lower concentration of such phase is present. Both materials show a clear absence of (crystalline) iron, but a major amorphous composition. The Kralingen sample also contains calcite, but, according to Figure 7, this

[2] partial vapour pressure of adsorbate gas in equilibrium with the surface at 77.4 K (b.p. of liquid nitrogen divided by the saturated pressure of the adsorbate gas

sample also consists of silica and the iron containing structure of Goethite (FeO(OH)). According to Nooijen [Nooijen, 1984] goethite is slowly formed from ferrihydrite, which may explain why the more concentrated Kralingen product contains more goethite than the Spannenburg material.

Table 2 lists the elements measured in three samples (Ferrosorp, Spannenburg and Kralingen) by the multi-element XRF technique. The fourth sample (Witharen) was analysed by Omegam Laboratories (data obtained by the Reststoffenunie). All four samples show a major contribution from iron. The iron content of the Witharen sample is notably lower than the iron content of the other samples. It is unknown what the other components in this sample may have been. However, during adsorption experiments it was noted that yellow coloured components were desorbed from the material, probably natural organic matter.

TABLE 2. QUANTITATIVE SUMMARY OF THE ELEMENTS ENCOUNTERED IN THE THREE IRON(HYDR)OXIDE SAMPLES BY X-RAY FLUORESCENCE. THE COMPOSITION OF THE WITHAREN SAMPLE WAS DETERMINED BY THE RESTSTOFFENUNIE.

| Element | Concentration of element in wt.% | | | |
|---|---|---|---|---|
| | Ferrosorp | Spannenburg | Kralingen | Witharen |
| Fe | 49.4 | 52.6 | 58.5 | 34.0 |
| Ca | 6.5 | 6.2 | 5.0 | 6.0 |
| Si | 5.7 | 5.1 | 2.3 | -- |
| Mg | 2.1 | 0.2 | 0.5 | 0.09 |
| P | 0.5 | 1.5 | 0.5 | 0.5 |
| Mn | 1.5 | 0.2 | 0.2 | 0.15 |
| Zr | 0.4 | 0.2 | 0.4 | -- |
| Ce | 0.2 | 0.1 | 0.3 | -- |
| Ba | 0.2 | 0.3 | < 0.1 | 0.035 |
| Al | 0.2 | < 0.1 | 0.2 | 0.05 |
| S | < 0.1 | 0.1 | 0.2 | -- |

From Table 2 it becomes clear that the majority of all samples consists of an iron containing phase, concentrations ranging from approximately 50-58 wt-%. All samples indeed display a substantial contribution from Ca (5-7 wt%), likely associated with the presence of the calcite phase as evidenced by the XRD investigations. One of the main differences among these samples are the relatively high contents of Mn and Mg in FerroSorp as compared to the other three samples. Apart from this, the elemental composition of Spannenburg material corresponds well with the FerroSorp composition, whereas the composition of the Kralingen material notably differs from both other iron(hydr)oxides.

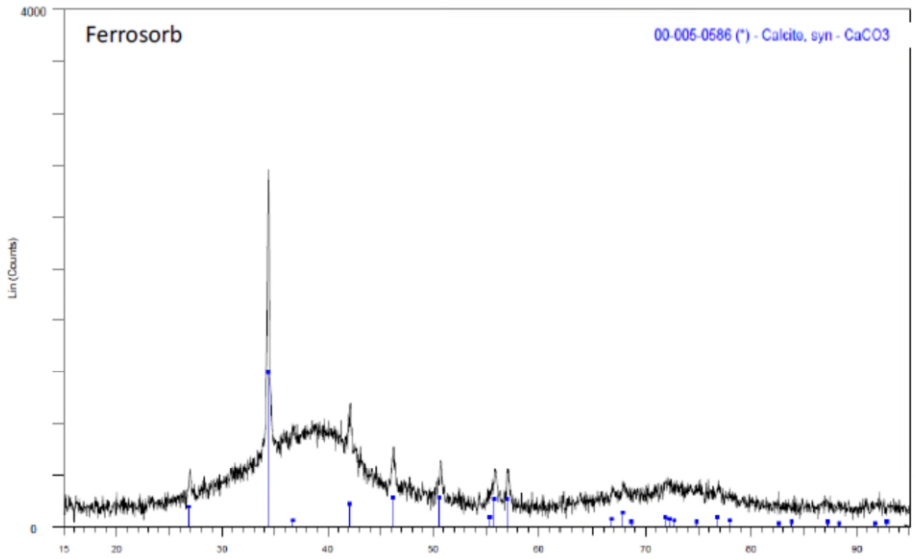


*Figure 5. Experimental and reconstructed XRD profiles of Ferrosorp*

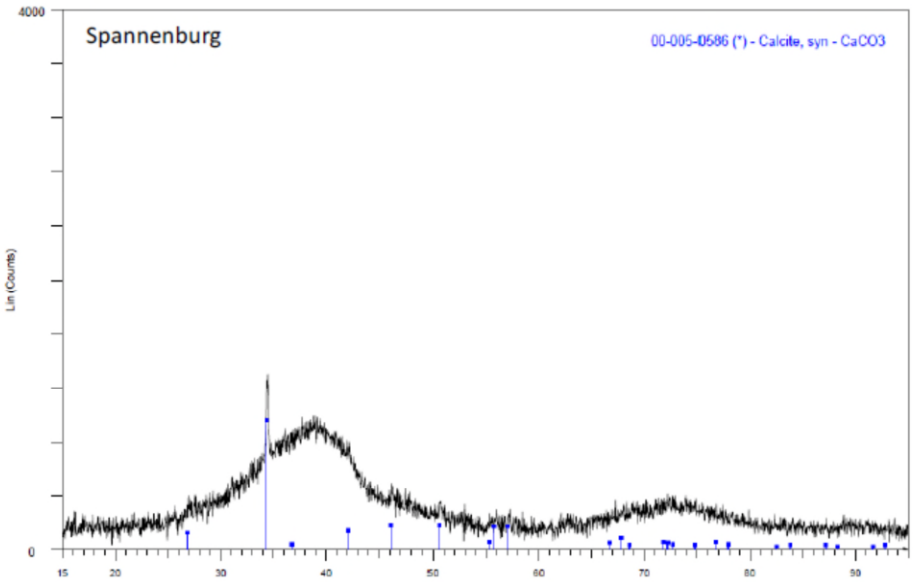


*Figure 6. Experimental and reconstructed XRD profiles of Spannenburg.*

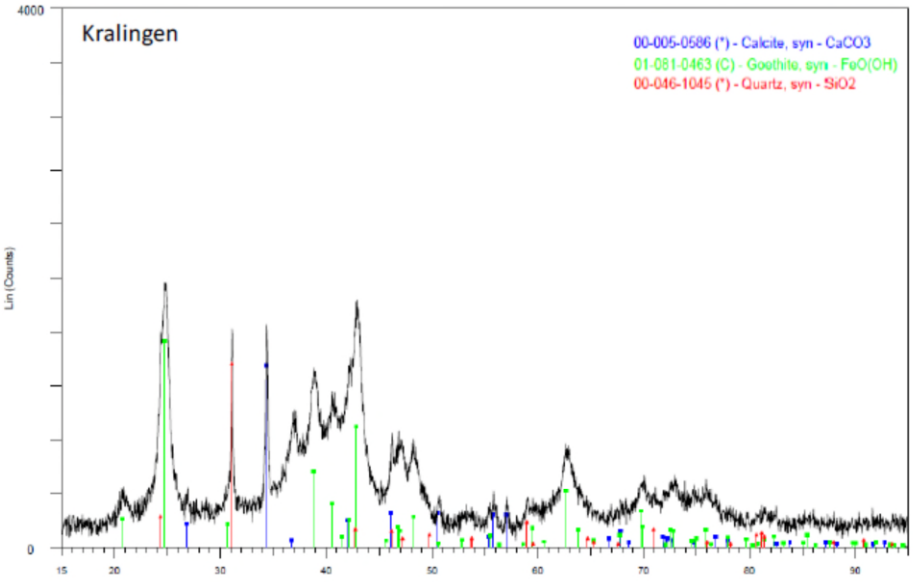


*Figure 7. Experimental and reconstructed XRD profiles of Kralingen.*

### 3.2.2 Pelletization of iron(hydr)oxides

After drying and sieving of the Spannenburg and Kralingen sludges particles in a size range of 0.6 to 1.4 mm were obtained. At first glance these particles did not seem to be very stable. Therefore three different binders were tested:

- Cebogel Bondex: a sodium bentonite specially modified for binding of pellets
- Cebogel IPR-012: a sodium bentonite specially modified for binding of pellets
- CMC (CAS 9004-32-4 Type Gabrosa P300D Batch/ID 2%Brf.9500mPa.s): carboxy methylcellulose, designed for binding of iron oxide pellets

Upon visual assessment it seemed that Cebogel IPR-012 gave more stable pellets than Cebogel Bondex, and therefore most experiments were carried out with pellets containing 1 or 2 wt-% of this material.

The textural properties of the pellets obtained are shown in Table 3.

TABLE 3. TEXTURAL PROPERTIES OF HET VARIOUS PELLETS AND THE STARTING MATERIAL

| Sample | $S_{BET}$ ($m^2/g$) | $V_{pore}$ ($cm^3/g$) | $V_{micro}$ ($cm^3/g$) | $S_{meso}$ ($m^2/g$) |
|---|---|---|---|---|
| Spannenburg | 230 | -- | -- | -- |
| Spannenburg with 2% bentonite | 231 | 0.385 | 0.075 | 84 |
| Kralingen | 117 | -- | -- | -- |
| Kralingen with 2% bentonite | 121 | 0.088 | 0.010 | 98 |
| Ferrosorp | 276 | 0.640 | -- | -- |

According to Table 3 the addition of bentonite does not affect the specific surface area $S_{BET}$. Thus, the surface available for phosphate adsorption does not have to change because of this treatment.

Another important parameter is the strength of the pellets. This was measured by means of the robotic compression tester, and the results of the Ferrosorp and Spannenburg/bentonite pellets are summarized in Table 4.

TABLE 4. CRUSHING STRENGTH AND PARTICLE SIZE DATA OBTAINED BY APPLICATION OF THE ROBOTIC COMPRESSION TESTER OVER THE SPANNENBURG/BENTONITE AND FERROSORP SAMPLES.

| | Ferrosorp | Spannenburg 0% bentonite | Spannenburg 1% bentonite | Spannenburg 2% bentonite |
|---|---|---|---|---|
| Number of measured particles | 50 | 50 | 50 | 50 |
| Average maximum force (N) | 5.8 | 2.7 | 1.6 | 2.0 |
| Standard deviation (N) | 3.5 | 1.7 | 0.7 | 1.1 |
| Average particle size ($\mu$m) | 2047 | 1065 | 1027 | 962 |
| Min particle size ($\mu$m) | 1155 | 694 | 690 | 626 |
| Median = D50 ($\mu$m) | 2048 | 1076 | 1018 | 975 |
| Maximum particle size ($\mu$m) | 2939 | 1341 | 1511 | 1318 |

Obviously, the average maximum force of the Spannenburg pellets is lower than for the Ferrosorp material. The addition of bentonite does not seem to increase this force, although visually the pellets seemed to be stronger.

A second test was carried out, using Spannenburg material pelletized with 1 wt% CMC. The "green pellets" thus obtained were heated to 500 ˚C or 800 C˚. In the first phase (heating until 500 ˚C) the organic material is believed to be burned, whereas somewhere in the second phase sintering of the iron oxides should occur. The results are shown in Table 5.

TABLE 5. CRUSHING STRENGTH AND PARTICLE SIZE DATA OBTAINED BY APPLICATION OF THE ROBOTIC COMPRESSION TESTER OVER THE SPANNENBURG/BENTONITE AND FERROSORP SAMPLES.

| | Spannenburg 105 ˚C | Spannenburg 500 ˚C | Spannenburg 800 ˚C |
|---|---|---|---|
| Number of measured particles | 50 | 50 | 50 |
| Average maximum force (N) | 3.3 | 3.7 | 10.5 |
| Standard deviation (N) | 1.5 | 2.1 | 5.0 |
| Average particle size ($\mu$m) | 1296 | 1080 | 1051 |
| Min particle size ($\mu$m) | 915 | 812 | 639 |
| Median = D50 ($\mu$m) | 1283 | 1070 | 1066 |
| Maximum particle size ($\mu$m) | 2939 | 1341 | 1511 |

According to Table 5 it can be concluded that the strength of the green pellets with CMC is higher than that of pellets produced with bentonite or without a binder. Furthermore, it can be seen that indeed between 500 and 800 ˚C sintering takes place, resulting in a strong increase in the crushing strength of the particles. The color of the material also turns from brown into red, and the volume seems to decrease about 40%. This is shown in Figure 8.

*Figure 8. Color of heated Spannenburg material with CMC: left sample heated at 800˚C, right sample heated at 500˚C*

### 3.2.3 Adsorption experiments

*Experiments with iron(hydr)oxides without binder material*
First some adsorption experiments were carried out with iron(hydr)oxides from both Spannenburg and Kralingen without any binder material. During these experiments it was found that the sample water should not contain any calcium, as this complexes with the phosphate, thus interfering with the adsorption results. Therefore, the results obtained with the pure material are not reported.

*Experiments with iron(hydr)oxides with bentonite*
Adsorption experiments were carried out in water not containing any calcium, using Spannenburg and Kralingen pellets made with 1 wt% bentonite. The results are shown in Figure 9 and Figure 10. Q is the phosphate load of the adsorbent, expressed as mg/g.

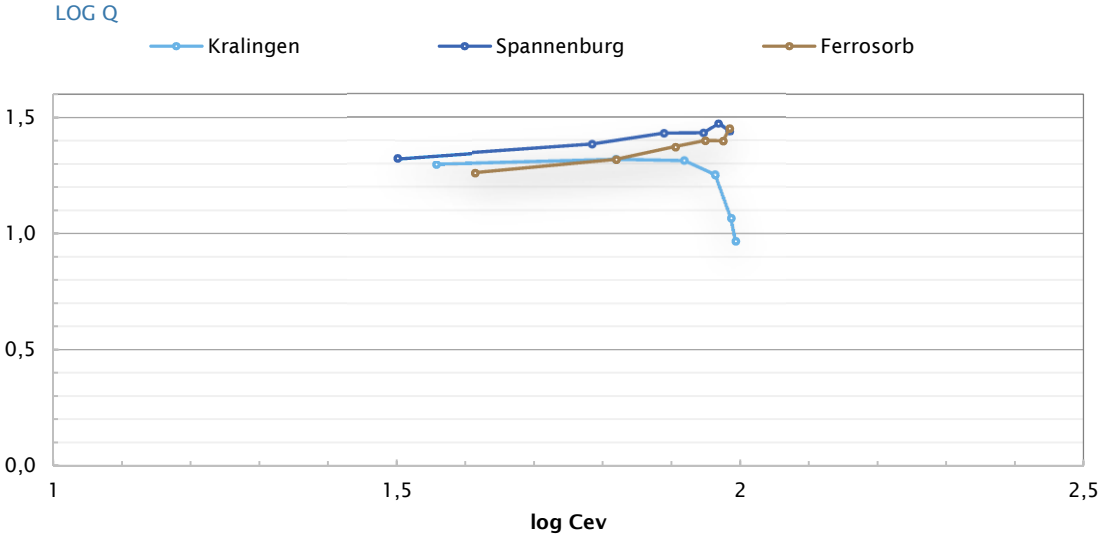


*Figure 9. Adsorption isotherm of Kralingen and Spannenburg material with 1wt% bentonite, and commercially available Ferrosorp.*

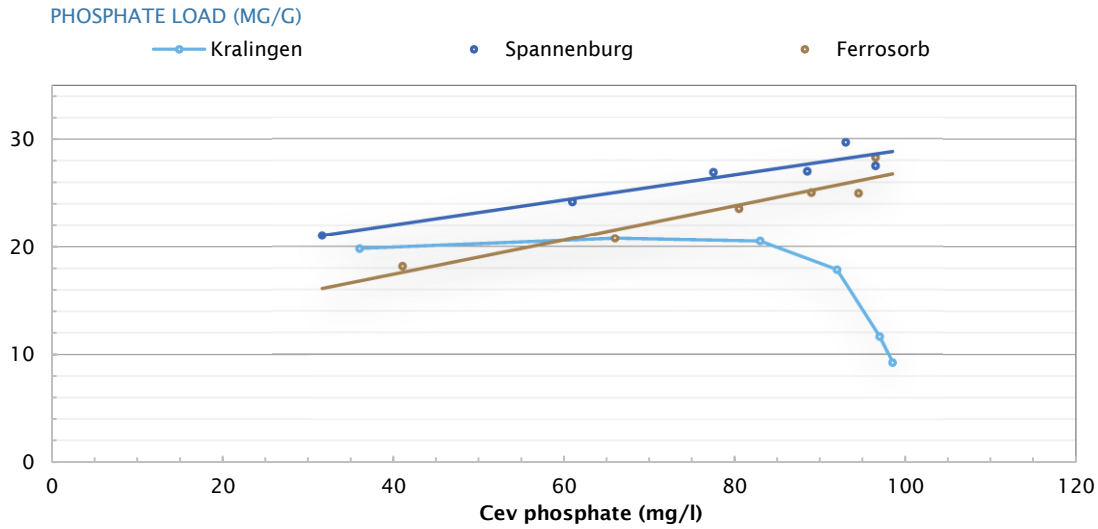


*Figure 10. Adsorption isotherm of Kralingen and Spannenburg material with 1wt% bentonite, and commercially available Ferrosorp.*

From these results it can be concluded that the Spannenburg material can adsorb about 20-30 mg phosphate/g, which is comparable, or even slightly better, than Ferrosorp. The Kralingen material shows a much lower adsorption of phosphate at lower dosages of adsorption material. This probably is related to the higher goethite content of this material, as from previous research it is known that goethite, contrarily to ironhydroxide or ferrihydrite ($Fe_5(O_4H_3)_3$), can hardly adsorb phosphate a [Nooijen, 1984; Stowa, 1994]. This may be related to either the crystal structure of goethite or to the fact that the specific surface area of goethite is much smaller than the surface area of amorphous material.

Adsorption experiments were also carried out with the Spannenburg material containing 1 % w/w CMC. The results are shown in Table 6.

TABLE 6. PHOSPHATE ADSORPTION AT CMC-TREATED AND HEATED PELLETS.

| Sample | mass (mg/l) | $PO_4$ (mg/l) | log($PO_4$) (-) | load (mg/g) | log(load) (-) |
|---|---|---|---|---|---|
| 105 ˚C | 1000 | 73.5 | 1.87 | 27.50 | 1.44 |
| 500 ° C | 1000 | 97.6 | 1.99 | 3.40 | 0.53 |
| 800 ° C | 1000 | 96.7 | 1.99 | 4.30 | 0.63 |
| Blank | 0 | 101 | 2.00 | | |

From these experiments it can be concluded that the adsorption of CMC and removal of moisture at about 100 ˚C does not significantly affect the amount of phosphate that can be adsorbed on the Spannenburg material. Obviously, the adsorption of CMC does not compete with phosphate adsorption. However, after heating of the sample to 500 ˚C or higher, the adsorption of the material appears to decrease notably. This is remarkable, as from Table 5 it can be concluded that heating to 500 ˚C hardly affects the pellet strength (in order to obtain a higher maximum force a higher temperature appears to be required). Obviously, crystallization already occurs before the pellet strength increases, resulting in a lower

phosphate adsorption. Pellet strength possibly is related to the degree of sintering of the iron oxide.

## 3.3 Conclusions

- In order to obtain stable pellets, a binder is required. Bentonite, which in literature often is applied, did not seem to be suitable in this project, but good results were obtained by using carboxymethyl cellulose.
- Amorphous iron(hydr)oxide has a larger specific surface area, and thus a higher phosphate adsorption capacity. Iron(hydr)oxide containing a substantial amount of crystalline material like goethite is much less effective for phosphate adsorption.
- Amorphous iron(hydr)oxides slowly crystallize at “room temperature”, and this process is accelerated at elevated temperatures. This means that “fresh” iron sludge should be used, consisting mainly of amorphous material. Besides, drying of the pellets should not be carried out at too high temperatures, in order to prevent crystallization. The preferred drying temperature for pellets is about 105 ˚C.
- In order to determine whether or not a certain iron sludge would be applicable for pellet formation and phosphate adsorption, the composition/crystallinity of the material can be determined. A simpler and cheaper way to determine the suitability may be by measuring the specific surface area ($S_{BET}$). As crystallization is accompanied by a significant decrease in surface area, this may be sufficient for practical applications.
- Iron(hydr)oxide pellets have an adsorption capacity of about 30 mg orthophosphate per g of iron(hydr)oxide.

# 4 Production scale-up

## 4.1 Introduction

To scale up production volumes of granular iron(hydr)oxides tests were done at two locations with capabilities for drying of sludges. The first location was at an agricultural biogas production facility in Biddinghuizen, the second was in a technical laboratory of Ebbens Engineering in Lochem. Ebbens is a supplier of drying equipment.

## 4.2 Scale-up at Biogas Plus, Biddinghuizen

The drying set-up in Biddinghuizen is part a manure fermentation plant. The biogas produced at this plant is fed into a combined heat and power plant. The heat is used by a nearby flower horticulture company and the electrical power is fed into the grid. A small part of the heat is used in a simple drying setup. The warm water is passing through a horizontal air heat exchanger. A blower is used to force the warm air along a steel trough containing the material to be dried (see Figure 11).

*Figure 11. Sludge drying set-up in Biddinghuizen*

The drying procedure consisted of mixing approximately 40-50 kg sludge (Spannenburg 8 % d.s.) with 2 % (m/m ds) CMC according to the recipe developed in the previous chapter. After

a few days the sludge was dried into a hard crust, which was grinded and sieved into the required fractions.

Because the set-up contains no measuring equipment, it was not possible to collect data on the recovery of usable product and energy demand. As the drying trough is limited to a volume of approx. 100 l sludge, the system has only a production capacity of a few kg. The procedure itself works quite easy and is suitable for testing larger batches. As a commercial production facility, this system is however not suitable. All materials used in the column test (see Chapter 5) were prepared in this way.

### 4.3 Scale-up at Ebbens, Lochem

The company Ebbens Engineering is a supplier of drying equipment. They own a test facility ('Technicum') to test different drying procedures on semi-technical scale, used to design and engineer industrial drying equipment. In this facility a more quantitative investigation on drying procedures was conducted.

The drying procedure proposed by Ebbens was based on a fluidized bed dryer, because it often results in a well-defined granular material. For iron sludge this procedure was never used so far. Therefore exact operating conditions were unknown.

First the sludge was dewatered by decanting or filtration. Decanting delivered the most suitable procedure. Because the decanted sludge is too wet to introduce into the fluidized bed dryer, a procedure was developed including drying sludge in an oven and grinding. Thus a dry seeding material was obtained, which was mixed with the liquid sludge, resulting in a dryable suspension. The seeding material was mixed with sludges from different procedures in order to optimize the dewatering procedure. Table 7 gives an overview of these sludges.

TABLE 7. DEWATERING TESTS AT EBBENS ENGINEERING (10 JANUARY 2014)

| Test | Purpose | Result |
|---|---|---|
| 1 | Pre-dewatering by decantation; CMC addition after dewatering | Dry solids content can be increased to 12 to 13 % |
| 2 | Pre-dewatering by filtration (Büchner); CMC addition after dewatering | Dry solids content can be increased to 22 to 23 % |
| 3 | CMC addition, before pre-dewatering by filtration (Büchner) | Dry solids content not determined. Filtration was more difficult than test 2 |
| 4 | Same as Test 1, but now on 6 buckets of sludge (total 29.5 kg sludge) | Sample for further drying tests |

Later, on January 24$^{rd}$ and 30$^{th}$ 2014, Ebbens conducted several drying tests with the fluidized bed dryer. The initial trial (test 1) was done by mixing dewatered sludge with seeding material dried in an oven. In the other tests, dry material from the previous test was used for mixing. Details of the drying tests are given in Annex 6.

This drying procedure resulted in 1,5 kg of material with a diameter between 0,425 and 1.25 mm, which was 67 % of the total material. Of the rest, 31 % was smaller than 0,425 mm and only 1 % was above 1.25 mm. The material was however too brittle for further column tests.

### 4.4 Adding further production capacity

For commercial production Reststoffenunie will need several tonnes of granular material in the first two years. In order to make these tonnes efficiently there is need for a larger

production site. The testing site at Biddinghuizen cannot provide this production capacity. Therefore, Reststoffenunie is looking for other options to increase the production capacity as required. Probably this can be found at locations where other goods are already dried at an industrial scale and waste heat is available for the drying process.

With the larger production capacity some operational problems may occur. For example the binding agent carboxymethyl cellulose (CMC) needs to be mixed with the iron sludge under high shear conditions. This is more difficult in large volumes, because of the increasing viscosity during mixing. Therefore a silo with proper stirring gear has to be available at the production site.

Furthermore, an iron sludge production site has to be selected, where iron sludges from different locations with different properties (viscosity, composition, solids content) can be mixed.

# 5 Column tests

## 5.1 Experimental

In Figure 12 a picture of the experimental set-up is given. Glass columns with an internal diameter of 3,5 cm were used for the column studies. The adsorption material is added to the columns as slurry in drinking water to prevent air occlusion in the bed of pellets. After reaching the desired bed height by tapping the column during filling, a reverse high flow is used to remove dust, air bubbles and column breakages. Also the column material is partly stratified in this manner. After settling of the material using down flow and again tapping of the column, the definitive desired bed height is reached by adding small amounts of adsorption material. The column containing the adsorption material, ready for use, remained under water during the experiment. The drinking water (Tull en 't Waal) used for the column experiments at high phosphate concentration (30 mg/L) was first treated with cation exchange resin (Lewatit Monoplus S100) removing $Ca^{2+}$ ions to prevent calcium phosphate formation. For the final column experiment with low phosphate dosage (addition of 3 mg $PO_4$/L) the used drinking water was not pretreated. Four experiments were carried out, as shown in Table 8.


*Figure 12. Experimental set-up for column experiments (right figure experiments 3 and 4)*

TABLE 8. EXPERIMENTAL CONDITIONS OF THE COLUMN TESTS.

| Column experiment | Sample (containing 2 wt% CMC, dried at 105 °C) | $C_0$ (mg $PO_4^{3-}$/L) | Column height (cm) | Flow (L/hour) | Contact time per cycle (min.) |
|---|---|---|---|---|---|
| 1 | Spannenburg | 30.50 | 76.5 | 5.7 | 7.7 |
| 2 | Spannenburg | 30.00 | 46.5 | 6.0 | 4.5 |
| 3 | Spannenburg | 3.00 | 43.5 | 1.25 | 20.0 |
| 4 | Witharen | 3.00 | 43.5 | 1.25 | 20.0 |

## 5.2 Results

### 5.2.1 Short contact time, high concentration

All experiments were carried out with iron oxide mixed with 2 wt-% CMC. In the first and second experiment iron from Spannenburg was used. It was noticed that the Spannenburg material gave a light yellow color to the water when the dispersion had stood without stirring for a while (see Figure 13). This yellow color is mainly caused by desorption of DOC, probably humic acids, as is shown by analyses of the effluent of Spannenburg. After one night of contact of the column material with drinking water, almost 200 mg DOC/L was (see Figure 14) desorbed from 220 g of adsorption material. The iron content in this sample was determined at about 2 mg Fe/L. The results of the column adsorption experiments are shown in Figure 14.

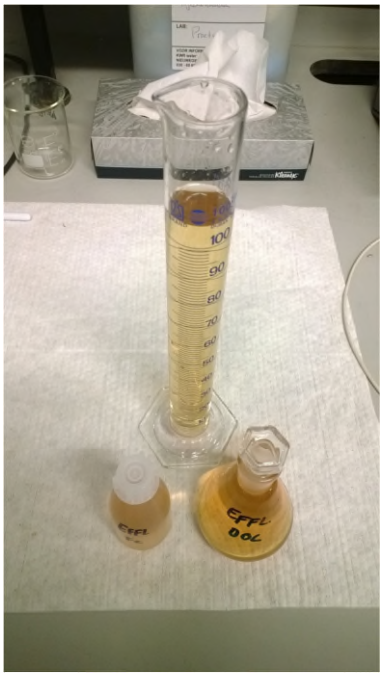


*Figure 13. Effluent of Spannenburg after two days standing still.*

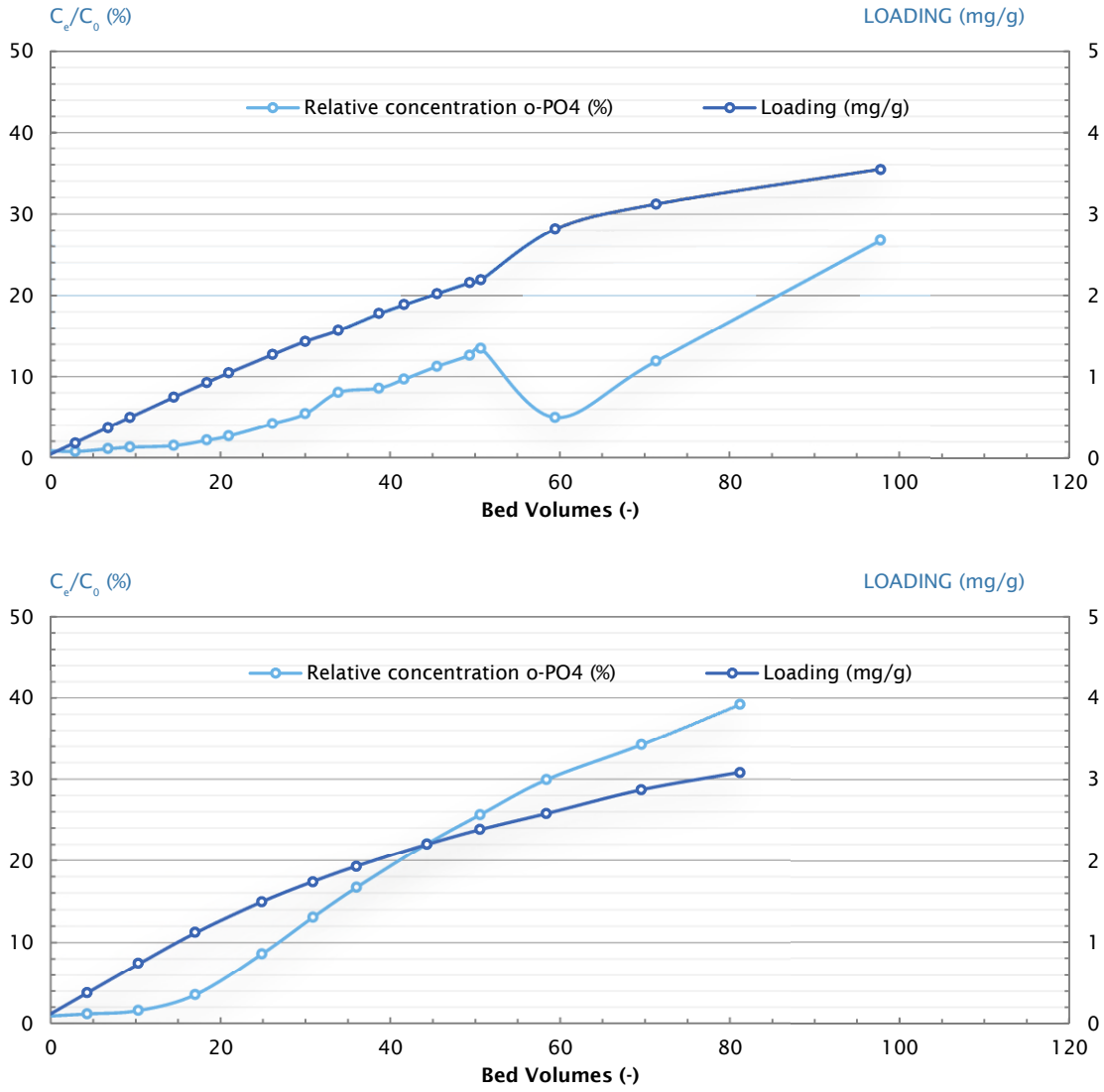


*Figure 14. Results of column experiments 1 (top) and 2 (bottom)*

It can be concluded that a phosphate load of about 30–40 mg/g can be obtained, and the adsorption kinetics are very quick. Even at a high flow and low contact time (of 7.7 or 4.5 min/cycle) the pellets show very effective adsorption of orthophosphate.

### 5.2.2 Long contact time, low concentration

In the third and fourth experiment two types of iron were applied: Spannenburg and Witharen. Some details on the Witharen material are shown in Table 9. As there appeared to be insufficient material from Witharen to fill the total column, about 1.5 cm on the top of the column had to be supplemented with Spannenburg material.

The Witharen material appeared to have a darker color than the Spannenburg material, and, most notably, its density appeared to be about 0.9 kg/L, whereas the Spannenburg material had a density of about 0.5 – 0.6 kg/L. The Witharen sample constantly emitted material with a yellow color. This yellow color probably also is caused by desorption of DOC, probably humic acids. As this sample has a notably lower iron content than for example the Spannenburg sample, and the analysis shows no other inorganic compounds, it is likely that this sample contains a relatively high amount of organic material.

A comparison of the physical properties of both Spannenburg and Witharen used in this study is given in Table 9. From this table it can be concluded that the Witharen sample has a significantly lower specific surface area, caused by the amount of micropores.

TABLE 9. PHYSICAL CHARACTERIZATION OF THE SPANNENBURG AND WITHAREN PELLETS, USED IN COLUMN EXPERIMENTS

| Sample | $S_{BET}$ ($m^2/g$) | $V_{pore}$ ($cm^3/g$) | $V_{micro}$ ($cm^3/g$) | $S_{meso}$ ($m^2/g$) | composition |
|---|---|---|---|---|---|
| Spannenburg 2% CMC | 230 | 0.385 | 0.075 | 84 | amorphous |
| Witharen 2% CMC | 73 | 0.162 | 0.008 | 56 | amorphous |

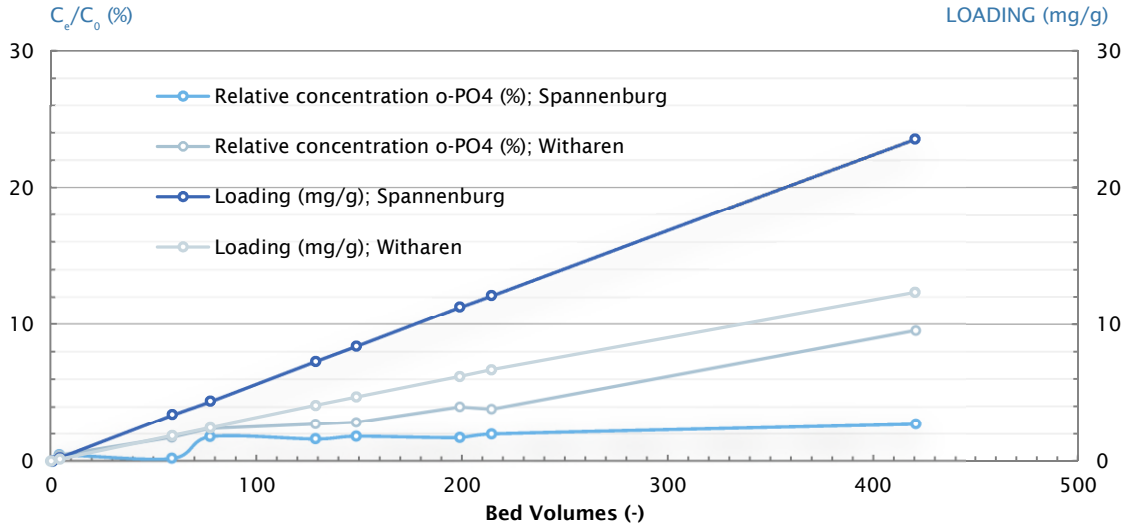


*Figure 15. Results of column experiments 3 and 4.*

From the column experiments 3 and 4 (Figure 15) it can be concluded that the Spannenburg material shows very good adsorption properties, even at low phosphate concentrations during a longer period of time. The material does not really seem to emit material into the water, and the pellets remain stable during handling (filling of the column) and operation. The Witharen material obviously has a much lower adsorption capacity for phosphate, which probably is related to the lower specific surface area of the material, as mentioned above.

## 5.3 Conclusions

The iron(hydr)oxide pellets, prepared from amorphous iron sludge using 2 wt-% CMC as a binder, show good results in column adsorption studies:

- Fast adsorption kinetics
- High phosphate adsorption capacity, both a high and low phosphate concentrations and at long and short contact times.
- Good stability of the pellets, even during longer operation periods.

Furthermore, it can be concluded that not only the crystallinity of a sample determines its suitability in phosphate adsorption, but probably mainly its specific surface area. Even Figure 15amorphous iron(hydr)oxide may have a lower pore volume and thus a lower surface area,

available for phosphate adsorption. This strongly favors determination of $S_{BET}$ in order to ascertain whether or not a certain iron sludge would be suitable for this application.

# 6 Regulatory and legal aspects

## 6.1 The Water Framework Directive: driving force for the market for granular iron(hydr)oxide

The main goal of the European Water Framework Directive (WFD) is to achieve a proper chemical and ecological state of all waters. The WFD consists of three parts:

- Make way for the fish
- Clean water
- Habitat recovery

Application of granular (hydr)oxide for phosphate removal contributes to the realisation of the WFD clean water goals, i.e. chemical and ecological good state. The labresults have shown that granular iron(hydr)oxide (from location Spannenburg) can be used to remove phosphate. Once business trials with granular iron(hydr)oxide will have proved its effectiveness in practice, water authorities can start to use the material for phosphate removal in surface water systems.

The water autorities are responsible for the water quality of the WFD waters (50% of the Dutch waters are WFD waters). Nevertheless, the Dutch government has the task to monitor the progress of water authorities in meeting the standards set in the WFD concerning contaminations. Not meeting the standards in time Can result in a fine for the Dutch government. "Possible penalties for the Dutch government, sanctioned on behalf of the European Commission for not implementing or not achieving the Water Framework Directive, are estimated to vary from EUR 25 000 to EUR 300 000 per day, and possible fines are estimated to vary from EUR 10 million to EUR 30 million" (Wienhoven et al., 2012).

In 2012 the Dutch government passed a law (Law: Compliance with European legislation public entities) which makes it possible to charge the water authority that does not comply with the WFD. This law creates an incentive for water authorities to improve surface water quality. Granular iron(hydr)oxide can help in this task by removing phosphate from surface water.

"Make way for the fish" is not directly related to application of granular iron(hydr)oxide, but it indirectly determines that its practical implementations should not block water streams or hinder fish migration. In other ways the dramatic reduction of phosphorus leads to a growth of aquatic plants. This growth makes it hard for fish to swim normally. Another problem created by the reduction of phosphorus, is a lack of nutrition for the fish. In general the Dutch sport fishing agency is against the removal of phosphorus from surface water, but if any product should be used, for the removal of phosphorus, they would prefer granular iron(hydr)oxide to be used, because the agency is regarding it as the best product available (Emmerik & Peters, 2014).

## 6.2 Legislation related to use and discharge of granular iron(hydr)oxide

The use of granular iron(hydr)oxide in surface water is subjected to the Dutch Water Act. According to this act, the introduction of substances into a waterbody is prohibited without a permit from the Minister (national water) or the water authority (regional water).

There is no standard for iron in surface water, only an indicative value MTT (maximum acceptated added value) of 96 µg/l diluted iron. The water authority has to make a judgement whether the application of iron(hydr)oxide is harmfull to the environment. The Dutch Helpdesk Water expects that water authorities will grant a permit because the positive effects on water quality will surpass any potentially negative effects. The regular permission procedure takes eight weeks.

For the application of granular iron(hydr)oxide in baskets or dikes there is a possible exemption from the permit obligation. Discharging water back in the same waterbody as it came from is permitted. If there is zero leakage from the pellets no permit is needed.

If granular irron(hydr)oxide is applied in a nature reserve the compentent nature authority or manager should be asked for permission as well. Depending on the situation a permit can be required.

Granular iron(hydr)oxide is subjected to the European Regulation on Registration, Evaluation, Authorisation and Restriction of Chemicals (REACH). Starting in 2018 manufacturers have to register their substances if the annual production is more than 1 ton (currently from 100 ton on). As the raw material is already registered and the material is not chemically modified, a separate registration for the granular material is not needed. The same goes for the byproduct of the production: iron-dust.

After use, granular iron(hydr)oxide is loaded with phosphate. If the product is not left in the environment but taken back, there are several end-use options. If the pellets are mixed with sand/sludge the material can be recycled as buildingmaterial after the required testing (AP04). Clean granular material can be used as raw material after receiving the ‘end of waste’ status according to the European Waste Directive. In future, phophate recovery and re-use of regenerated granular iron(hydr)oxide may be feasible, e.g. using anaerobic conditions. The legal aspects of this recovery need further study.

### 6.3 Dutch Law and regulations

If Reststoffenunie starts the production of granular iron, additional legislative constraints have to be considered. The most important one is the Working Conditions Act (ARBO wet). The manufacturer has to keep in mind the regulations concerning iron dust, because it may be formed during production.

The implementation of the WFD in the Netherlands is going slowly, because the Dutch government has not taken a clear position yet. The Government at least want to achieve the goals set by the WFD, but to achieve the main goal of good water condition more strict standards may have to be set (OECD Studies on Water, 2014). These mixed answers complicate the progress in the next few years concerning the WFD goals in the Netherlands. But Europe is pushing the members of the European union to achieve the WFD goals. Not meeting the WFD-criteria in the end may result in the EU forcing the member states to pay penalties. So it is likely that the Dutch government will meet these standards. Figure 16 shows which waters in the Netherlands do not meet the WFD.

One of the reasons Dutch water authorities are waiting to comply with the WFD, is the runoff of phosphorus from agriculture. The Dutch government adopted a law, named the Van der Vlies resolution. “In this resolution, it is laid down that the Dutch agricultural sector shall not be burdened with an increase in costs when measures have to be taken for the implementation of the WFD, i.e. has made it impossible to force farmers to incur additional costs when implementing the WFD.” (OECD Studies on Water, 2014).

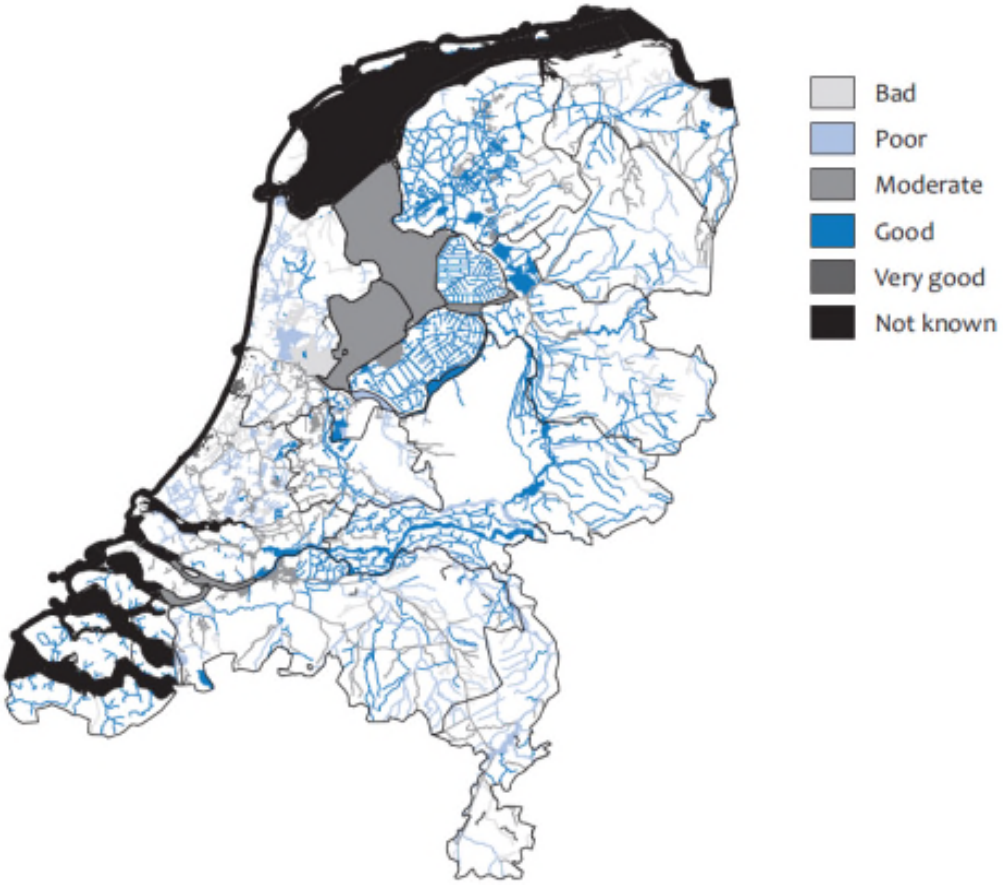


*Figure 16. Categorisation of Dutch waters on phosphorus concentrations (OECD Studies on Water, 2014)*

# 7 Environmental aspects

## 7.1 Environmental impact

The biggest environmental impact is the drying of iron sludge into a solid matter. To reduce the environmental effects, drying should be done by using waste heat, e.g. available at biodigesters. Often these installations have excess heat available that is only partly used in the digester or for drying manure. Sometimes it is used for the heating of nearby greenhouses.

Sludge drying takes energy to heat the sludge to the evaporation temperature and to evaporate water (latent heat). Heating of sludge depends on the temperature difference and the specific heat of the sludge. The latent heat of evaporation of water is 2,260 kJ/kg. This means that for drying 1 $m^3$ of sludge (8 % d.s.) at 100 ˚C, approximately 380 MJ is required for heating (from 10 to 100 ˚C) and 2,260 MJ for evaporating the water, in total 2,640 $MJ/m^3$ sludge or 33 MJ/kg granular material. The related greenhouse gas emission is 150 kg $CO_2$ per $m^3$ sludge or 1.9 kg $CO_2$/kg granular material. These figures show that it is essential to use waste heat for the production process of the granular material.

TABLE 10. CALORIC VALUE AND GREEN HOUSE GAS EMISSIONS BY NATURAL GAS AND BIOGAS.

| Gas type | Caloric value $MJ/m^3$ | $CO_2$-emission $kg/m^3$ |
|---|---|---|
| Natural gas | 31.65 | 1.8 |
| Biogas | 23.40 | 1.3 |

The product itself has no negative impact on the environment. The iron sludge used as raw material for the production of granular iron(hydr)oxide has low levels of contamination and the binding agent that is added to the iron sludge, is chosen because of its eco friendliness and its binding capacity.

There is one other factor that has an impact on the environment, this is the transport of iron sludge. As iron sludge only consist of 8% dry matter, this means that large amounts of water are transported. But by using the “GRID-model” (Model used to pick a most cost/mileage efficient location) the transport distances can be optimized. In this way Reststoffenunie is able to keep the environmental impact as low as possible.

Table 11 gives a summary of different environmental aspects for granular iron(hydr)oxide and its competitors, concerning: use of raw materials, P-adsorption capacity and contaminations/substances present in the product. For more detailed information please see Appendix VII. Lanthanum concentration in fish, product sheet Ferrosorp and contaminations Ferrosorp and dried iron sludges.

TABLE 11. COMPARING GRANULAR IRON(HYDR)OXIDE (GIH) TO BIGGEST COMPETITORS

| | **Granular iron(hydr)oxide** | **Ferrosorp plus** | **Phoslock** | **GEH 104** |
|---|---|---|---|---|
| Emissions | | Higher levels of contamination (As, Ni, see Appendix | Release of Lanthanum, which can cause environmental damage | Emissions during production synthetic iron(hydr)oxide. |
| Resource depletion | No use of raw materials | No use of raw materials | Adding of the rare earth metal: Lanthanum<br>Use of raw materials | Use of raw materials |
| Energy/$CO_2$ | Usage of surplus heat from a biodigester to dry iron sludge reducing the mileage driven with iron sludge using the "GRID-Model" | | | Expensive applications, needs a lot of energy<br>Energy intensive production.<br>Much residual moisture in the final product, which leads to unnecessary mileage |
| Efficiency | | Similar P-adsorption capacity as GIH (KWR-tests) | Lower P-adsorption capacity as GIH | |

# 8 Supply chain viability

## 8.1 Potential markets and market volumes

To determine the market potential of granular iron(hydr)oxide, first the current value chain of (wet) iron sludge was evaluated. Figure 17 shows the current value chain, mainly consisting of iron sludge transport. Two pathways have to be distinguished: the iron sludge either goes directly to a customer (most of the time, iron sludge has to have more than 8% dry matter), or sludge is stored in a silo where the dry solids content can be increased.

The cost for transport per 1000 kg of iron sludge with 8% dry matter delivered directly to a customer are about €10 per ton sludge (€ 120 per ton dry matter). When Reststoffenunie sells wet iron sludge directly to an end user, it receives a revenue of €13 per ton sludge (or €160 per ton dry matter) which leaves a profit of about €3 per ton sludge. Selling it via a silo leads to the same revenue, but the costs are about € 25 per ton sludge, leading to a loss of €12 per ton sludge. In practise, around two third is transported directly to customers and one third is transported via a silo. Table 12 presents the costs and revenues for this situation. Overall, this corresponds to a loss of about € 2 per ton sludge or € 20 per ton dry matter.

TABLE 12; COSTS AND REVENUES FOR CURRENT IRON SLUDGE VALUE CHAIN (€ PER TON DRY MATTER)

| | Transport costs to silo (€/t) | Cost silo (€/t) | Transport costs to customer (€/t) | Total costs (€/ton) | % direct and via silo | Overall costs/revenues (€/t) |
|---|---|---|---|---|---|---|
| **Supply direct to consumer** | | | - 120 | -120 | 67% | - 180 |
| **Supply via silo** | - 120 | - 60 | - 120 | -300 | 33% | |
| **Sales** | | | | | | + 160 |
| **Net sales value** | | | | | | - 20 |

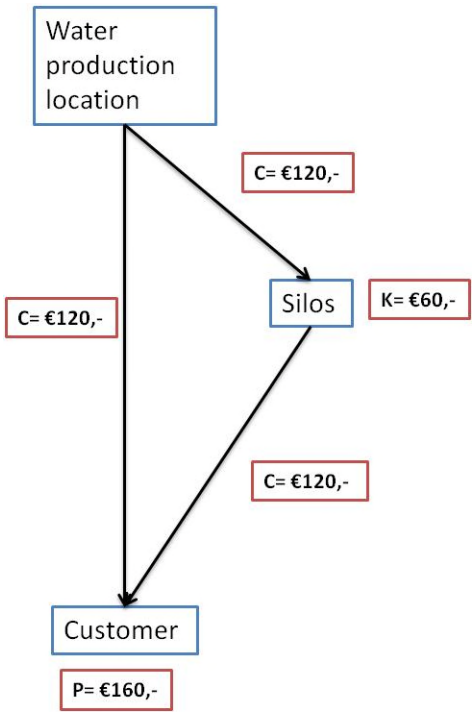


*Figure 17. Simplified current value chain (C = cost, P = revenue): Iron sludge process view with costs and revenues (per ton dry matter).*

To produce one ton of granular iron (hydr)oxide, between 10 and 15 tons of wet iron sludge is used (8 % dry solids). Because the available or produced sludge is fixed in The Netherlands, this means that if sludge would be used for production of granular iron(hydr)oxide, less sludge can be sold directly. This would lead to a reduction of the revenues of Reststoffenunie of €160 per ton dry matter. However, the costs are reduced as well with € 180 per ton dry matter (Figure 17). Therefore, the business case for producing and selling granulated sludge should be compared to a current case where the net costs are 20 € per ton dry matter.

The cost for the making of granular iron (hydr)oxide consist of three parts: transport costs from the water treatment plant to manufacturing facility, costs raw materials (iron sludge and CMC) and processing costs (sludge drying, milling, sieving and packaging). The research of the supply chain viability of the granular iron (hydr)oxide shows that the revenues are higher than the costs.

# 9 Conclusions and recommendations

## 9.1 Conclusions

The experimental research has shown that wet iron containing sludge can be converted into a granular iron (hyrdr)oxide that is suitable for phosphate removal from surface water. A recipe for production using CMC as a binder material gives a granular material that is strong enough to use it as a filter medium.

The phosphate adsorption capacity strongly depends on its origin and composition of the iron sludge. Also storage time before drying is an important factor. To create a material with a high adsorption capacity, freshly produced sludge is required. The iron(hydr)oxides should be amorphous and the material requires a high specific surface area. As crystallinity increases the material loses its adsorption capacity.

Column experiments have indicated fast adsorption kinetics, high phosphate adsorption capacity (both at high and low phosphate concentrations and at long and short contact times) and good stability of the pellets, even during longer operation periods. For quality control measurement of the BET specific surface area is proposed.

Reststoffenunie will be able to enter new profitable markets with the product. These markets can assure three very important issues for Reststoffenunie:

1. They are able to make a profit.
2. They can guarantee sales to their suppliers (drinking water companies).
3. They can spread the risks for the drinking water companies, the more market segments Reststoffenunie is able to sell to, the lower the risk.

In addition to the before mentioned issues, there are also very promising developments on the market. E.g. the market is still developing and additional growth is expected, creating extra sales opportunities. These signals are:

1. Approaching deadline of the Water Framework Directive (WFD)
2. Penalties for not implementing/achieving the WFD
3. Closing the Phosphate cycle is of increasing importance for the farmers
4. The market is waiting for a good product, when there is a good product the market will improve
5. Granular iron(hydr)oxide is expected to be an effective treatment material for removing other contaminations such as heavy metals and arsenic from water or hydrogensulfide from biogas.

There are also a few developments which have to be watched closely because they can have a positive but also negative impact on the improvement of the market. An example is the increasing attention for fish within the WFD. The Dutch sport fishing agency said that they are against the removal of phosphate. But they also mentioned that, when water authorities have to remove phosphate, that they prefer the use of granular iron(hydr)oxide for treatment.

## 9.2 Recommendations

Based on the findings of this research it is recommended to continue with the development of granular iron(hydr)oxide production. The most important next step is to create an energy efficient production line and find ways to realize and control a constant product quality. Also other aspect of the supply chain, such as selecting and supplying sludges, transporting them to the production facilities and the selling process have to be organised.

# 10 References

Abouzeid, A.Z.M., Seddik, A.A. (1981). Effect of iron ore properties on its balling behaviour. Pow. Technol. 29, 233-241

Arai, Y., Sparks, D.L. (2001). ATR-FTIR spectroscopic investigation on phosphate adsorption mechanisms at the Ferrihydrite-water interface. J. Coll. Int. Sci. 241, 317-326

Cong, H., Yu, B. (2011). Fabrication of superparamagnetic macroporous Fe3O4 and its derivates using colloidal crystals as templates. J. Coll. Int. Sci. 353, 131-136

Dammann, E., Benzinger, S. (1995). Verwertung von Eisenhydroxidschlämmen aus der Grundwasseraufbereitung in der kommunalen Abwasserbehandlung. Schlußbericht zum Forschungsvorhaben Förderkennzeichen 02 WT 9329/2, Bundesministerium für Forschung und Technologie.

Emmerik, W. v., & Peters, J. (2014, April 16). Relatie KRW en Sportvisserij. (O. v. Kolk, & J. Elings, Interviewers)

Fan, X.-H., Gan, M., Jiang, T., Chen, X.-L., Yuan, L.-S. (2011). Decreasing bentonite dosage during iron ore pelletising. Ironmaking and Steelmaking 38 (8), 597-601

Joosten, K. (2004). Drinking water sludge; applicability of iron sludge from drinking water purification for fixation of S and P in wastewater treatment plants. Master Thesis University of Utrecht.

Kawatra, S.K., Ripke, S.J. (2003). Laboratory studies for improving green ball strength in bentonite-bonded magnetite concentrate pellets. Int.J.Miner. Process. 72, 429-441

Koch, D. (2002); Bentonites as a basic material for technical base lines and site encapsulation cut-off walls; Apll.Clay Sci., 21 (1-2), 1-11

Koopmans, G.F., Chardon, W.J., Groenenberg, J.E. (2010). Karakterisatie van ijzerslib en –zand; een verkenning van dem ogelijkheden van het gebruik van deze reststoffen om fosfaatverliezen vanuit landbouwgronden naar het oppervlaktewater te verminderen. Alterra-rapport 2047

Luo, S.d, Yi., C., Zhou, Y. (2011). Direct reduction of mixed biomass-Fe2O3 briquettes using biomass-generated syngas. Renewable Energy 36, 3332-3336.

Mao, Y., Pham, A.N., Xin, Y., Waite, T.D. (2012). Effects of pH, floc age and organic compounds on the removal of phosphate by pre-polymerized hydrous ferric oxides. Sep. Pur. Technol. 91, 38-45

Milne, C.J., Kinniburgh, D.G>, van Riemsdijk, W.H., Tipping, E. (2003). Generic NICA-Donnan model paramters for metal-ion binding by humic substances. Environ. Sci. Technol., 37, 958-971

Mohamed, O.A., Shalabi, M.E.H., El-Hussiny, N.A., Khedr., M.H., Mostafa, F. (2003). The role of normal and activated bentonite on the pelletization of barite iron ore concentrate and the quality of pellets. Pow. Technol. 130, 277-282

Noijen, W.F.J. (1984). De microstructuur van ijzerhydroxideslib; Karakterisering van coagulatieslib dat vrijkomt bij de zuivering van oppervlaktewater en de huidige bedrijfsvoering van droogbedden. Afstudeerverslag TUD.

Ogblonlowo, D.B. (1989). Comparison of some synthetic resins with bentonite as binders for blast-furnace pellet production. Min.Eng. 2 (1), 131-136

OECD Studies on Water. (2014). Water Governance in the Netherlands, fit for the future? http://dx.doi.org/10.1787/9789264102637-en: OECD Publishing.

Pan, B., Wu, J., Pan, B., Lv, L., Zhang, W., Xiao, L., Wang, X., Tao, X., Zheng, S. (2009). Development of polymer-based nanosized hydrated ferric oxides (HFOs) for enhanced phosphate removal from waste effluents. Wat.Res. 43, 44421-4429

Persson, P., Nilsson, N., Sjöberg, S. (1996). Structure and bonding of orthophosphate ions at the iro oxide-aqueous interface. J. Coll. Int. Sci. 177, 263-275

Qiu, G., Jiang, T., Li, H., Wang, D. (2003). Functions and molecular structure of organic binders for iron ore pelletization. Coll. Surf. A Physicochem. Eng. Asp. 224, 11-22

Sadakane, M., Horiuchi, T., Kato, N., Sasaki, K., Ueda, W. (2010). Preparation of three-dimensionally ordered macroporous perovskite-type lanthanum-iron-oxide LaFeO3 with tunable pore diameters: high porosity and photonic property. J. Sol. State Chem. 183, 1365-1371

Shu, M., Yin, H., Liu, G. (2012). Influences of bentonite modification methods on the physical and chemical properties of bentonite. Adv. Mat. Res. 482-484, 2096-2102

Sivrikaya, O., Arol, A.I., (2011). Pelletization of magnetite ore with colemanite added organic binders. Powder Technol. 201, 23-28

Sivrikaya, O., Arol, A.I., (2012). The bonding/strengthening mechanism of colemanite added organic binders in iron ore pelletization; Int. J. Min. Proc. 110-111, 90-100

STOWA 1994, Toepassing van drinkwaterslib op rioolwaterzuiveringsinrichtingen; STOWA 1994-12

Tugrul, N., Derun, E.M., Psikin, M. (2007). Utilization of pyrite ash wastes by pelletization process. Powder Technol. 176, 72-76

Vimonses, V., Lie, S., Jin, B., Chow, C.W.K., Saint, C. (2009). Kinetic study and equilibrium isotherm analysis of Congo Red adsorption by clay minerals; Chem.Eng.J., 148 (2-3), 354-364

Voortman, H., van den Heuvel, P. (2002). Haalbaarheidsstudie VASIM-proces

Weng, L., Temminghoff, E.J.M., Lofts, S., Tipping, E., van Riemsdijk, W.H. (2002). Complexation with dissolved organic matter and solubility control of heavy metals in a sandy soil. Environ. Sci. Technol., 36, 4804-4810

Weng, L., Van Riemasdijk, AW., Hiemstra, T. (2008). Humic nanoparticles at the oxide-water interface: interactions with phosphate ion adsorption. Envrion.Sci.Technol. 42, 8747-8752

Wienhoven M., Briene M., van der Velde R., van den Boomen R., de Vries S. (2012), Bekostiging waterbeheer, Wie betaalt welk deel van de EU KRW?, Opdrachtgever: DG Ruimte en Water. Uitvoering: Ecorys, Witteveen + Bos, Centrum voor Omgevingsrecht en -beleid.

Zach-Maor, A., Semiat, R., Shemer, H. (2011). Adsorption-desorption mechanism of phosphate by immobilized nano-sized magnetite layer: interface and bulk interactions. J. Coll. Int. Scie. 363, 608-614

Zhou, Q., Wang, X., Liu, J., Zhang, L. (2012). Phosphorus removal from wastewater using nano-particulates of hydrated ferric oxide doped activated carbon fiber prepared by sol-gel method. Chem. Eng.J. 200-202, 619-629

Patent applications

WO 02/26630 A1 (2002)

WO 02/26630 A1(2002)

EP 1 344 564 A2 (2003)

EP 1 328 476 B1 (2001)

EP 1 328 478 B1 (2001)

EP 1 582 505 B1 (2005)

# Appendix I

## Analysis of Ferrosorp and starting materials Spannenburg and Kralingen

### $N_2$ adsorption

Prior to the $N_2$ adsorption measurements, the samples were degassed in vacuum at 90°C for 16 h. The dry sample weight obtained after the pre-treatment has been used in the various calculations. Adsorption and desorption isotherms with $N_2$ as adsorptive were then recorded at 77 K on a Micromeritics TriStar 3000.

In N2 physical gas adsorption, the sample cell holding the outgassed sample is evacuated and cooled to liquid nitrogen temperature (77 K). Portions of nitrogen are dosed into the sample cell and will be partly adsorbed on the surface, eventually getting into equilibrium with the gas phase. In this way adsorption and desorption points are recorded at different pressures and the ad- and desorption isotherm can be constructed.

Adsorbed nitrogen will first form a quasi-monolayer on the sample surface while further increase in pressure results in the formation of multilayers. In the region where monolayer and multilayers are formed, the specific surface area ($S_{BET}$) is determined according to the BET (Brunauer, Emmet and Teller) theory. This model is applicable to non-porous and meso- and macroporous materials and adsorption points in the relative pressure range between 0.05 and 0.25 are typically used [1]. In case mesopores are present in the sample under investigation, $N_2$ will condense in these pores at higher relative pressures. This information can be used to derive a mesopore size distribution, typically by means of the BJH pore size model [2-3]. Besides, the empirical t-plot methodology can be used to discriminate between contributions from micropores and remaining porosity (i.e. mesoporosity, macroporosity and external surface area contributions) [4].

### Mercury intrusion porosimetry

Mercury intrusion porosimetry (MIP) measurements are performed on a variety of samples to determine the pore volume, porosity, and the pore size distribution. This technique is based on the principle that mercury is a non-wetting liquid and requires a force to penetrate voids.

In a typical analysis, pressures from approx 0.01 kPa to 200 MPa are applied and application of the Washburn equation [1] converts the pressure to pore diameter ($d_{pore}$) according to the following relationship:

$$d_{pore} = \frac{-4\gamma cos\theta}{p}$$

A value of 140° is used for the contact angle ($\theta$), as this has proven to be a realistic value for most oxidic materials [5], while the surface tension of mercury ($\gamma$) amounts to 480 dyne/cm. Measurement of the volume displacement by the solid sample also enables to

assess its density. In a typical experiment, the contributions from pores covering the range of approximately 800 micrometers down to 5 nanometers can be assessed quantitatively.

The MIP experiment over the Ferrosorp sample has been carried out on a Micromeritics Autopore 9505 porosimeter in the pressure range from vacuum up to 220 MPa. Prior to the measurement, the sample has been pre-treated in an oven at 90°C for 16 h. The dried sample was then transferred and weighed in the sample holder. Approximately 0.35 grams of dry sample has been used in the analysis and the dry sample weight has been used in the various calculations.

### X-Ray Diffraction

The atomic and molecular structure can be attained by X-ray diffraction investigations. Crystalline atoms cause diffraction of an X-ray beam into specific directions, leading to typical reflections at certain characteristic positions in the XRD profile. In that way, the presence of crystalline matter can be identified; amorphous matter typical results in very broad, ill-defined reflections.

The X-ray powder diffraction (XRPD) patterns were recorded in a Bragg-Brentano geometry in a Bruker D5005 diffractometer equipped with Huber incident-beam monochromator and Braun PSD detector. Data collection was carried out at room temperature using monochromatic Cu radiation (K$\alpha$1 $\lambda$ = 0.154056 nm) in the 2$\theta$ region between 15° and 95°, step size 0.035 degrees 2$\theta$.

The sample, of about 30 milligrams, was deposited on a Si <510> wafer and was rotated during measurement. Data evaluation was done with the Bruker program EVA.

### X-Ray Fluoresence

The chemical composition of the various samples has been investigated by means of the multi-element technique X-Ray Fluorescence (XRF). X-ray fluorescence is a non-destructive analysis for the qualitative and semi-quantitative determination of elements with an atomic weight ≥ carbon (Z ≥ 6). X-ray fluorescence is based on the principle that an atom is irradiated by high-energetic radiation and releases an electron from a valence shell of the atom. A higher placed electron takes the vacant place and transmits element-characteristic radiation. The intensity of this radiation is a guideline for the concentration of the concerned element.

Semi-quantitative determination of the multi-element composition of the three samples has been attained in a PANalytical Axios-Max XRF spectrometer. Prior to the analysis, the three samples were milled followed by drying in an oven at 90°C. Subsequently, a suitable pellet has been generated by means of pressing about 1.5 g of the powdered sample with boric acid without binder; this assists in homogenization of the sample and it minimizes matrix effects.

### Crushing strength

The robotic compression tester (RCT) is an instrument for measuring the strength of particles and granules with limited supervision.

The robotic compression tester measures the maximum crushing force of individual particles or granules. The crushing force of particles with sizes ranging from 500 µm to ≈ 5000 µm can be measured. About 40 up to 100 particles are placed on a 2 cm thick smooth finely polished stainless steel plate and the coordinates of each particle and size are determined by a CCD camera. Consecutively all particles at the known coordinates are crushed and the

required force is measured with a quartz force transducer. The transducer is a device that uses the piezoelectric effect to measure pressure, acceleration, strain or force by converting them to an electrical charge. The sensitive transducer is suitable for measuring quasi-static and dynamic tensile and compressive forces ranging from a few mN to 100 N.

The principal result of the compression test is an average maximum crushing force and the particle size distribution. Compressive strength of particles and agglomerates is often proportional with the particle diameter, the relationship is generally in the form: L = k Dn where L is the crushing force, D is the particle diameter, k and n are constants depending on the material.

### Results & Discussion:

The $N_2$ adsorption and desorption isotherms of the Ferrosorp sample and a part of the adsorption isotherm of the Spannenburg and Kralingen samples are depicted in Figure 18 and Figure 19. It can be seen that in the relative pressure (partial vapour pressure of adsorbate gas in equilibrium with the surface at 77.4 K (b.p. of liquid nitrogen divided by the saturated pressure of the adsorbate gas) range of approx. 0.05-0.25 different volumes of nitrogen have been adsorbed for the three samples. This indicates a different surface area available for adsorption since in this pressure range the monolayer capacity is obtained, which is used to calculate the BET surface area. Table 13 indeed confirms that the BET surface areas are dissimilar for the three samples: the Kralingen sample exhibits the lowest surface area of 117 $m^2 g^{-1}$, which is only half compared to the Spannenburg sample (SBET = 230 $m^2g^{-1}$). The Ferrosorp sample clearly presents the highest BET area of 276 $m^2 g^{-1}$ [4].

In case of sample Ferrosorp, the full adsorption and desorption isotherms have been recorded to attain additional information on the porosity/pore structure. The isotherm suggests a highly mesoporous sample with a rather well-defined pore size distribution as concluded from the hysteresis loop that progresses almost vertical with rather parallel branches and a plateau at higher relative pressure. This is further confirmed by the pore size distribution derived from the adsorption branch and displayed in Figure 19, evidencing pore in the range from 2-90 nm with a mode at 40 nm. It could be questioned whether the well-defined pore structure is the result of the original sludge, a specific particle size fraction, or whether this has been obtained by the addition of some additive/binder.

TABLE 13. TEXTURAL PROPERTIES OF THE VARIOUS SAMPLES INVESTIGATED AS DERIVED FROM THE $N_2$ ADSORPTION EXPERIMENTS INCLUDING THE WEIGHT LOSS OBTAINED UPON VACUUM PRE-TREATMENT

| Sample | Weight loss wt% | $S_{BET}$ $m^2/g$ | $V_{pore}$ $cm^3/g$ |
|---|---|---|---|
| Ferrosorp | 27.9 | 276 | 0.640 |
| Spannenburg | 16.8 | 230 | n.m |
| Kralingen | 6.3 | 117 | n.m |

The mercury intrusion curve obtained over sample Ferrosorp is displayed in Figure 20 (top). Two distinct steps can be discerned: the first step at low pressure is associated with filling of the voids among the individual particles and obviously depend on the particle morphology and particle size (inter-particle porosity). Since the particles are relatively large, the step occurs at relatively low pressures (p << 0.1 MPa) correlating with relatively large voids. Then only at pressures higher than 30 MPa, a relatively sharp intrusion starts related to the filling of the pores inside the particles (intra-particle porosity). This second step progresses until

the highest pressure reached (220 MPa), which relates to the filing of the smallest pores than can be measured with this technique (approx. 5 nm pore diameter).

The pore size distribution in Figure 20 (bottom) indeed confirms two different contributions; the contribution centred around 500 micrometers due to the filling of the interparticle voids and a contribution centred around 20 nm (span 6 nm – 90 nm) associated with the filling of the intra-particle pores. The latter contribution is qualitatively in excellent agreement with the pore size distribution derived from the $N_2$ adsorption investigations. The total pore volume for the intra-particle contribution is 0.53 $cm^3\ g^{-1}$, which is approximately 15% lower than the total pore volume value derived from $N_2$ adsorption. This difference can be explained by the fact that the mercury intrusion is not capable of measuring and quantifying pores < approx. 6 nm and from $N_2$ adsorption is becomes clear that such pores are present in the Ferrosorp sample (and thus measured by – and included in the results of – the $N_2$ adsorption analysis).

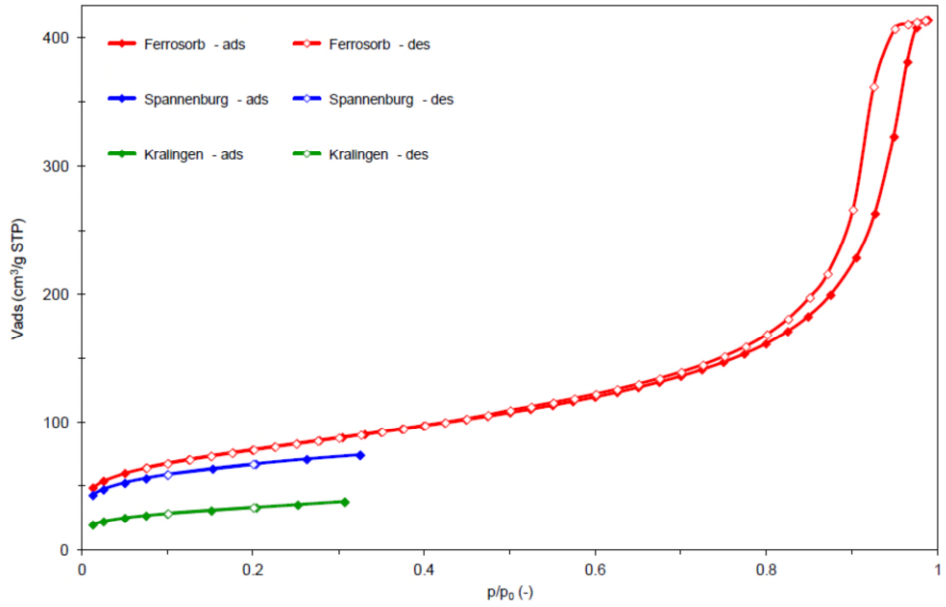


*Figure 18. $N_2$ adsorption and desorption isotherms at 77 K of the Ferrosorp sample and part of the adsorption isotherms of the Spannenburg and Kralingen sample. Closed symbols denote adsorption, open symbols denote desorption.*

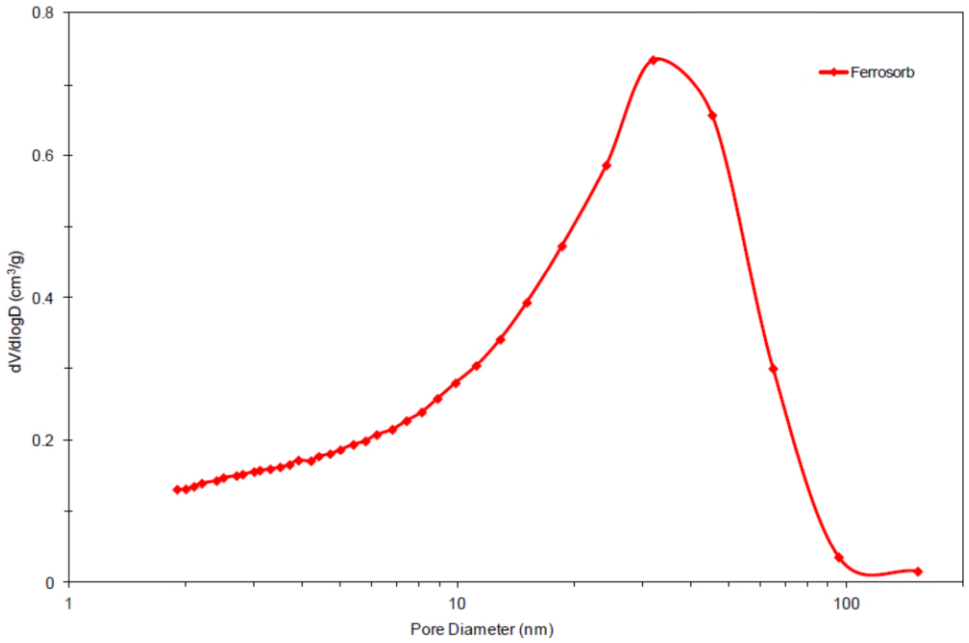


*Figure 19. BJH pore size distribution of the Ferrosorp sample derived from the adsorption branch of the isotherm in Figure 18.*

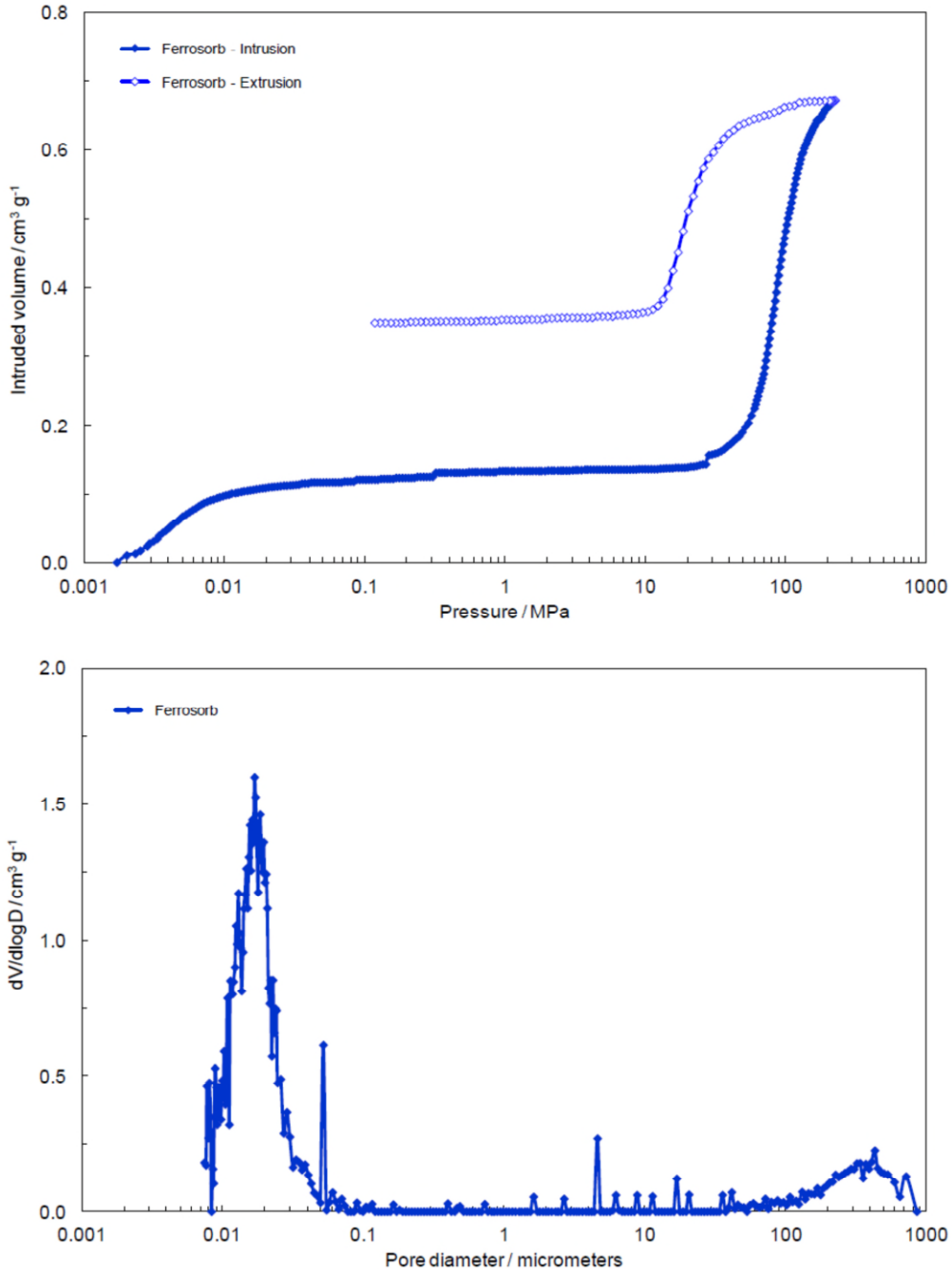


*Figure 20. Mercury intrusion and extrusion curve obtained over sample Ferrosorp (top) and the pore size distribution derived from the intrusion curve (bottom).*

In Figure 21, the XRD patterns of the three samples are shown. From this comparison it becomes clear that distinct similarities as well as differences are found among the three samples. The Ferrosorp reference sample presents mostly broad amorphous contributions with one strong reflection at around 35° 2-theta. Application of the structure identification database ICDD pdf4 reveals that this contribution, coupled to other weaker contributions, should be assigned to the presence of a so-called calcite ($CaCO_3$) phase (see Figure 22, top). The colored lines in Figure 21 show the peak positions and intensities of the identified

phases, such as found using the ICDD pdf4 database. No other distinct patterns associated with the presence of iron can be distinguished in sample Ferrosorp.

The same characteristic reflection at 35° 2-theta can also be found in both samples Kralingen and Spannenburg, related to the presence of calcite. The Spannenburg sample (Figure 22, middle) also presents a mostly amorphous structure with one contribution previously assigned to calcite and as such appears to have a similar structure as the Ferrosorp sample. Compared to the Ferrosorp sample, however, this calcite contribution tends to have a much lower intensity in the Spannenburg sample and thus a lower concentration of such phase would be present.

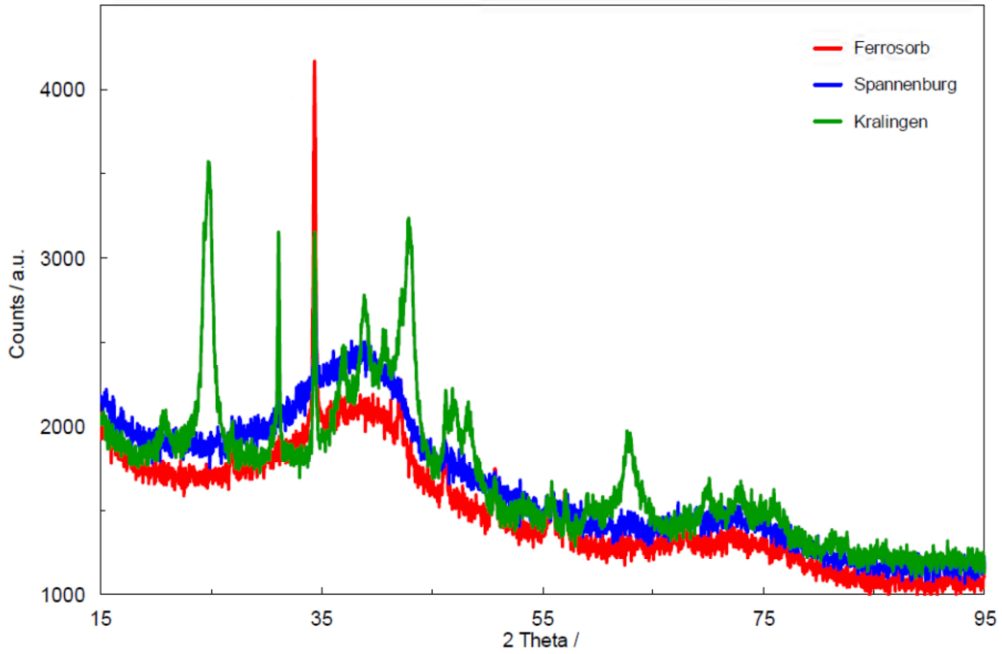


*Figure 21. XRD patterns of the three samples investigated.*

Finally, Figure 22 (bottom) shows that besides the calcite contribution, the Kralingen sample also contains other contributions that can be assigned to silica (SiO2) and the iron-containing structure of Goethite (FeO(OH)) and as such clearly has a different crystalline composition compared to the other two samples. Interestingly, the Ferrosorp and Kralingen samples show the apparent absence of (crystalline) Fe although a major amorphous contribution can be observed in all samples as derived from the broad contribution around 40° 2-Theta. X-ray fluorescence should confirm the presence of iron and other elements in the various samples.

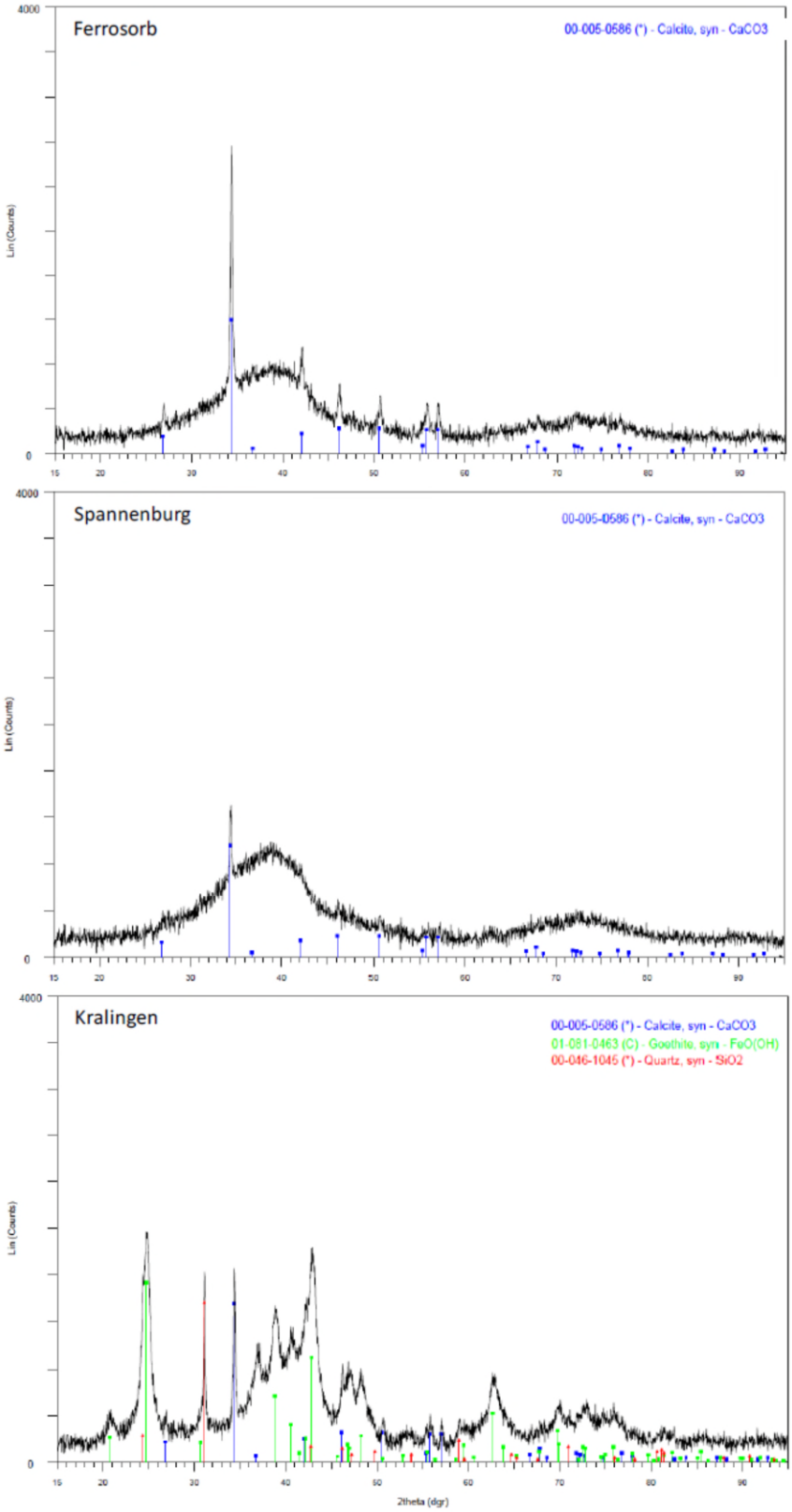


*Figure 22. Experimental and reconstructed XRD profiles of Ferrosorp (top), Spannenburg (middle) and Kralingen (bottom).*

Table 14 lists the elements measured in the three samples by the multi-element XRF technique and this overview shows a major contribution from iron in all samples.

TABLE 14. QUANTITATIVE SUMMARY OF THE ELEMENTS ENCOUNTERED IN THE THREE IRON(HYDR)OXIDE SAMPLES BY X-RAY FLUEORESCENCE

| Element | Concentration of element in wt.% | | |
|---|---|---|---|
| | Ferrosorp | Spannenburg | Kralingen |
| Fe | 49.4 | 52.6 | 58.5 |
| Ca | 6.5 | 6.2 | 5.0 |
| Si | 5.7 | 5.1 | 2.3 |
| Mg | 2.1 | 0.2 | 0.5 |
| P | 0.5 | 1.5 | 0.5 |
| Mn | 1.5 | 0.2 | 0.2 |
| Zr | 0.4 | 0.2 | 0.4 |
| Ce | 0.2 | 0.1 | 0.3 |
| Ba | 0.2 | 0.3 | < 0.1 |
| Al | 0.2 | < 0.1 | 0.2 |
| S | < 0.1 | 0.1 | 0.2 |

From Table 14 it becomes clear that the majority of all samples consists of an Fe-containing phase, concentrations ranging from approx. 50-58 wt.%. All samples indeed display a substantial contribution from Ca (5-7 wt.%), likely associated with the presence of the Calcite phase as evidenced by the XRD investigations. One of the main differences among the three samples is a relatively low content of Si in the Kralingen sample, whereas the Ferrosorp sample contains a relatively high content of Mn and Mg as compared to the other two samples. Possibly Mn and Mg are important elements in the foreseen application?

Finally, the strength of the Ferrosorp particles has been studied by the robotic compression tester and the results obtained have been summarized in Figure 23 and Table 15. Overall the particles break at a rather low force of on average 6 N with some single extreme values of 15 N and 21 N (Figure 23, top and Table 15). The particle size of the entities studied ranges from approx. 1 mm to 3 mm (Figure 23, bottom).

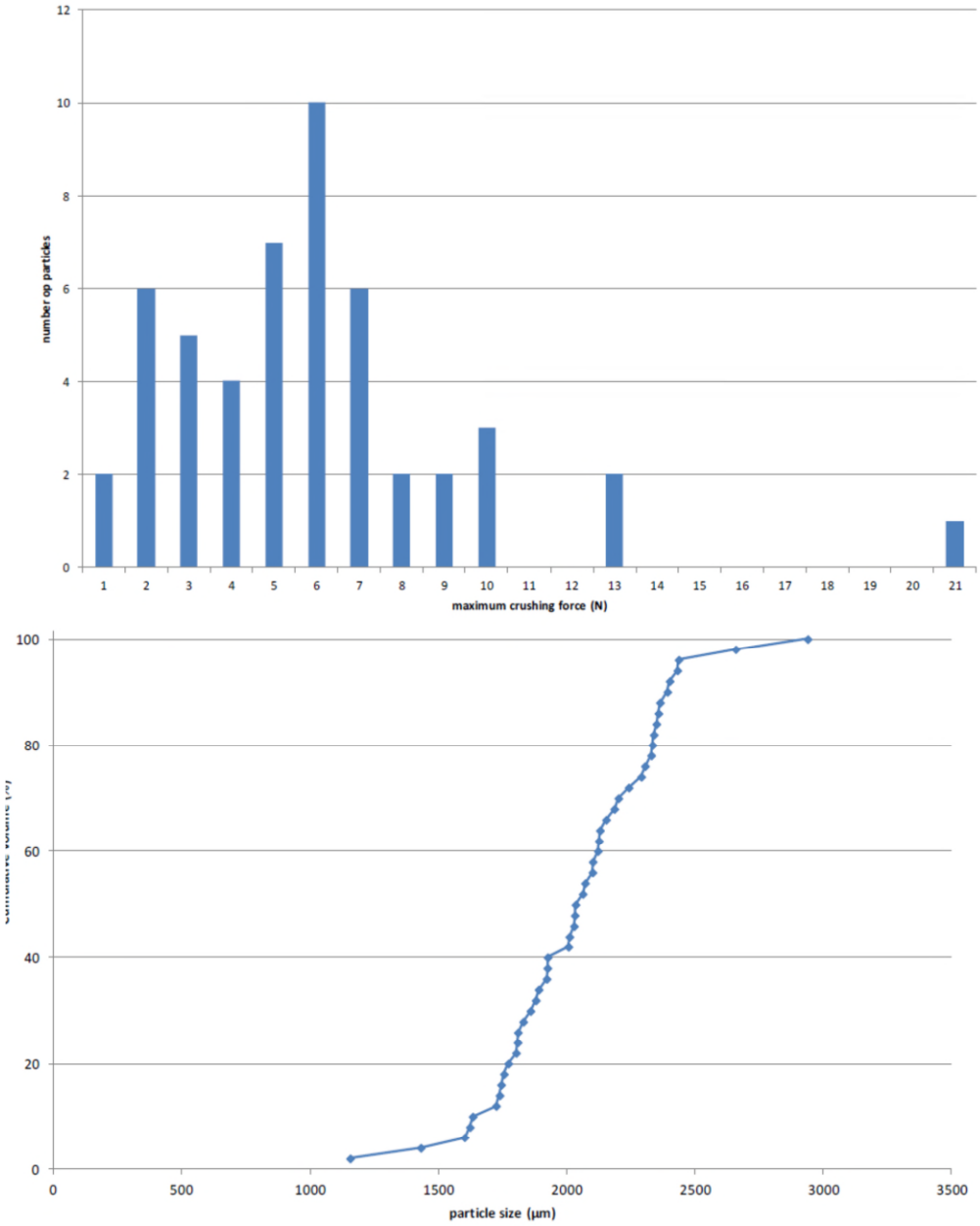


*Figure 23. Number of particles breaking at a specific crushing strength (top) and the cumulative particle size distribution of the Ferrosorp particles that have been studied for their crushing strength (bottom).*

TABLE 15. CRUSHING STRENGT HAND PARTICLE SIZE DATA OBTAINED BY APPLICATION OF THE ROBOTIC COMPRESSION TESTER OVER THE FERROSORP SAMPLE.

| | **Ferrosorp** |
|---|---|
| Number of measured particles | 50 |
| Average maximum force (N) | 5.8 |
| Standard deviation (N) | 3.5 |
| Average particle size (µm) | 2047 |
| Min. Particle size (µm) | 1155 |
| Median = $D_{50}$ (µm) | 2048 |

## References

[1] S.J. Gregg, K.S.W. Sing, “Adsorption, Surface Area and Porosity”, 2nd ed., Academic Press, London, 1982.

[2] E.P. Barret, L.G. Joyner, P.H. Halenda, J. Am. Chem. Soc. 73 (1951) 373.

[3] J.C. Groen, L.A.A. Peffer, J. Pérez-Ramírez, Microporous Mesoporous Mater. 60 (2003) 1.

[4] B.C. Lippens, J.H. de Boer, J. Catal. 4 (1965) 319.

[5] J.C. Groen, J. Pérez-Ramírez and L.A.A. Peffer, in: F. Rodriguez-Reinoso, B. McEnaney, J. Rouguerol, K.K. Unger (Eds.) “Incorporation of appropriate contact angles in textural characterization by mercury porosimetry”, Characterization of Porous Solids VI, Studies in Surface Science and Catalysis, Vol. 144, Elsevier, Amsterdam, 2002, pp. 91-98.

# Appendix II

## Analysis of Spannenburg and Kralingen materials with bentonite

### $N_2$ adsorption

Prior to the $N_2$ adsorption measurements, the samples were degassed in vacuum at 90°C for 16 h. The dry sample weight obtained after the pre-treatment has been used in the various calculations. Adsorption and desorption isotherms with $N_2$ as adsorptive were then recorded at 77 K on a Micromeritics TriStar 3000.

In $N_2$ physical gas adsorption, the sample cell holding the outgassed sample is evacuated and cooled to liquid nitrogen temperature (77 K). Portions of nitrogen are dosed into the sample cell and will be partly adsorbed on the surface, eventually getting into equilibrium with the gas phase. In this way adsorption and desorption points are recorded at different pressures and the ad- and desorption isotherm can be constructed.

Adsorbed nitrogen will first form a quasi-monolayer on the sample surface while further increase in pressure results in the formation of multilayers. In the region where monolayer and multilayers are formed, the specific surface area ($S_{BET}$) is determined according to the BET (Brunauer, Emmet and Teller) theory. This model is applicable to non-porous and meso- and macroporous materials and adsorption points in the relative pressure range between 0.05 and 0.25 are typically used.[1] In case mesopores are present in the sample under investigation, $N_2$ will condense in these pores at higher relative pressures. This information can be used to derive a mesopore size distribution, typically by means of the BJH pore size model.[2-3] Besides, the empirical t-plot methodology can be used to discriminate between contributions from micropores and remaining porosity (i.e. mesoporosity, macroporosity and external surface area contributions).[4]

### X-Ray Diffraction

The atomic and molecular structure can be attained by X-ray diffraction investigations. Crystalline atoms cause diffraction of an X-ray beam into specific directions, leading to typical reflections at certain characteristic positions in the XRD profile. In that way, the presence of crystalline matter can be identified; amorphous matter typical results in very broad, ill-defined reflections.

The X-ray powder diffraction (XRPD) patterns were recorded in a Bragg-Brentano geometry in a Bruker D5005 diffractometer equipped with Huber incident-beam monochromator and Braun PSD detector. Data collection was carried out at room temperature using monochromatic Cu radiation (Kα1 λ = 0.154056 nm) in the 2θ region between 15° and 95°, step size 0.035 degrees 2θ.

The sample, of about 30 milligrams, was deposited on a Si <510> wafer and was rotated during measurement. Data evaluation was done with the Bruker program EVA.

### Crushing strength

The robotic compression tester (RCT) is an instrument for measuring the strength of particles and granules with limited supervision.

The robotic compression tester measures the maximum crushing force of individual particles or granules. The crushing force of particles with sizes ranging from 500 µm to ≈ 5000 µm can be measured. About 40 up to 100 particles are placed on a 2 cm thick smooth finely polished stainless steel plate and the coordinates of each particle and size are determined by a CCD camera. Consecutively all particles at the known coordinates are crushed and the required force is measured with a quartz force transducer. The transducer is a device that uses the piezoelectric effect to measure pressure, acceleration, strain or force by converting them to an electrical charge. The sensitive transducer is suitable for measuring quasi-static and dynamic tensile and compressive forces ranging from a few mN to 100 N.

The principal result of the compression test is an average maximum crushing force and the particle size distribution. Compressive strength of particles and agglomerates is often proportional with the particle diameter, the relationship is generally in the form: $L = k\,D^n$ where $L$ is the crushing force, $D$ is the particle diameter, $k$ and $n$ are constants depending on the material.

### Results & Discussion:

The $N_2$ adsorption and desorption isotherms of the "Spannenburg 2% Bentonite" and "Kralingen" sample are depicted in Figure 24. It can be seen that in the relative pressure range of approx. 0.05-0.25 different volumes of nitrogen have been adsorbed for the two samples. This indicates a different surface area available for adsorption since in this pressure range the monolayer capacity is obtained, which is used to calculate the BET surface area. Table 16 indeed confirms that the BET surface areas are dissimilar for the samples: the "Kralingen" sample exhibits the lowest BET surface area of 121 $m^2\,g^{-1}$, which is only half compared to the "Spannenburg 2% bentonite" sample ($S_{BET}$ = 231 $m^2\,g^{-1}$).

The isotherm of the "Kralingen" sample suggests that the sample predominantly contains mesopores around 4 nm, as the small hysteresis loop is forced to close at p/p0 ≈ 0.40-0.45. The plateau at higher relative pressures indicates that the sample does not possess any large pores. In parallel, it can be concluded that the "Spannenburg 2% bentonite" sample does possess larger pores, as the isotherm displays an increased uptake at higher relative pressures, corresponding to the filling of such larger pores.

The pore size distribution in Figure 25 indeed confirms that sample "Spannenburg 2% bentonite" has larger pores but it also shows that this sample contains micropores, since the size distribution rises at pores < 2 nm. The "Kralingen" sample almost exclusively possesses small mesopores. The size distribution of this sample has a mode centred around 3 nm and almost no porosity above 10 nm. The sample also seems to contain some micropores < 2 nm.

TABLE 16. TEXTURAL PROPERTIES OF THE VARIOUS SAMPLES INVESTIGATED INCLUDING THE WEIGHT LOSS OBTAINED UPON VACUUM PRE-TREATMENT.

| Sample | Weight loss wt% | $S_{BET}$ $m^2/g$ | $V_{pore}$ $cm^3/g$ | $V_{micro}$ $cm^3/g$ | $S_{meso}$ $cm^3/g$ |
|---|---|---|---|---|---|
| Spannenburg 2% bentonite | 1.9 | 231 | 0.385 | 0.075 | 84 |
| Kralingen | 2.7 | 121 | 0.088 | 0.010 | 98 |

It can be concluded from Table 16 that the specific surface area of sample "Spannenburg 2% bentonite" is mostly generated by the micropores in the samples. Almost two-third of the surface area is due to this microporosity. This comes from the fact that at a certain volume smaller pores have greater contributions to the surface area than larger pores.

Table 16 also shows that the "Kralingen" sample has some minor microporosity. However, the small mesopores are the main reason that this sample still has a relatively high surface area of 121 $m^2 g^{-1}$.

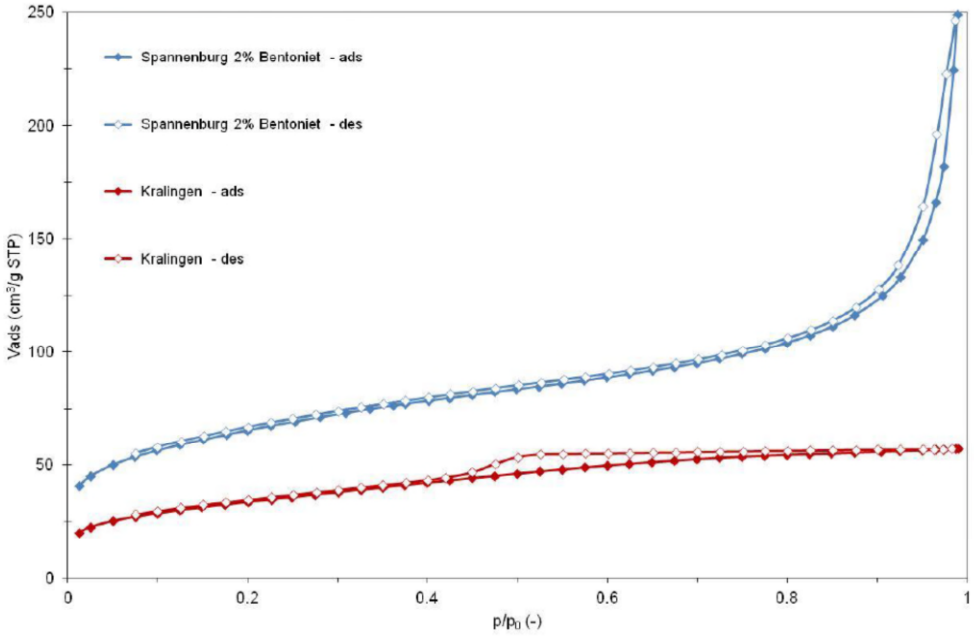


*Figure 24. $N_2$ adsorption and desorption isotherms at 77 K of the "Spannenburg 2% bentonite" and "Kralingen" sample. Closed symbols denote adsorption, open symbols denote desorption.*

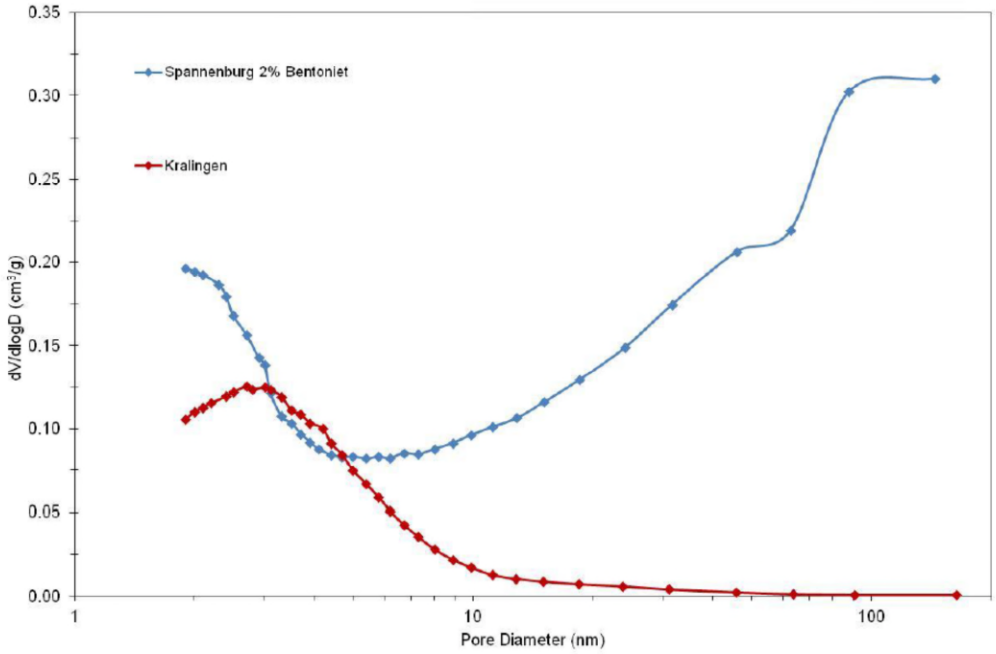


*Figure 25. BJH pore size distribution of the "Spannenburg 2% bentonite" and "Kralingen" sample derived from the adsorption branch of the isotherms in Figure 24.*

In Figure 26, the experimental and reconstructed XRD patterns of the "Kralingen" sample are shown. The phase identification shows that both the iron-containing Goethite phase and calcite are encountered in this "Kralingen" sample, similar to the Kralingen sample that has been previously characterized.

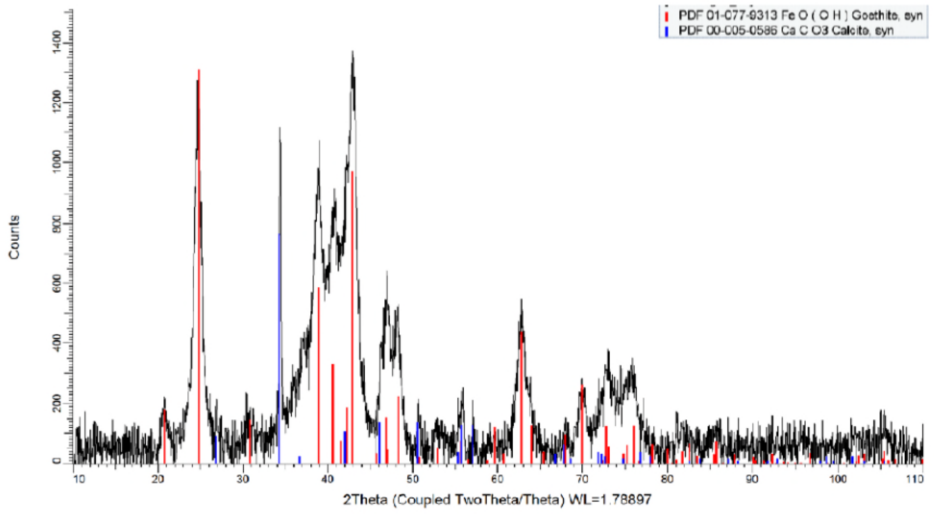


*Figure 26. Experimental (black line) and reconstructed XRD (red and blue lines) profiles of the Kralingen sample.*

Finally, the strength of the various Spannenburg particles has been studied by means of the robotic compression tester and the results obtained have been summarized in Figure 27 to Figure 32 and Table 17. From the graphical and tabular data it becomes evident that the particles show a relatively low crushing strength in the range from approx. 1.5 - 2.7 N.

It appears that the addition of Bentonite (either in 1% or 2%) does not significantly alter the crushing strength of the Spannenburg particles.

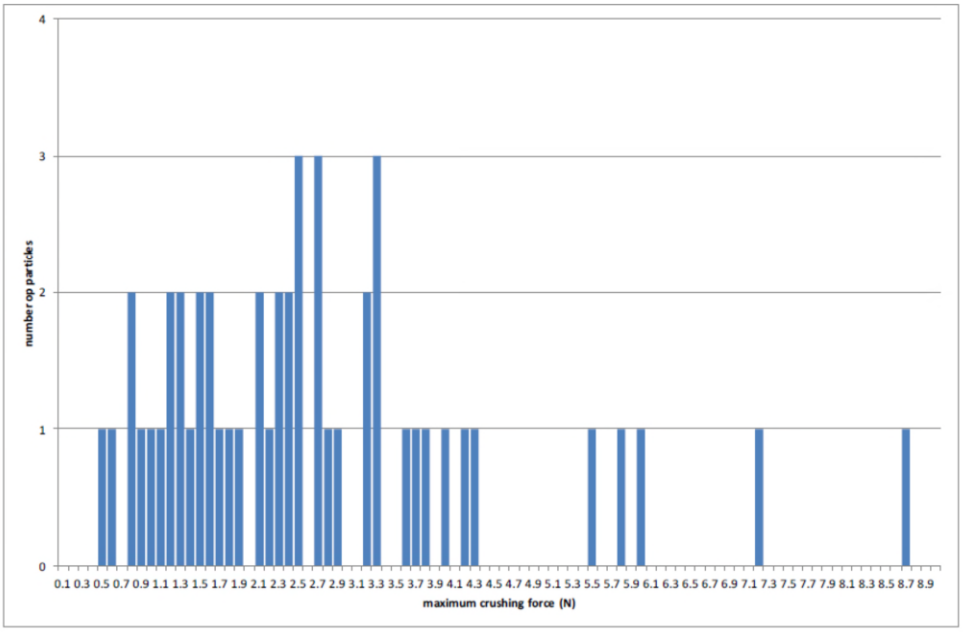


*Figure 27. Number of particles breaking at a specific crushing strength of sample "Spannenburg 0% Bentonite".*

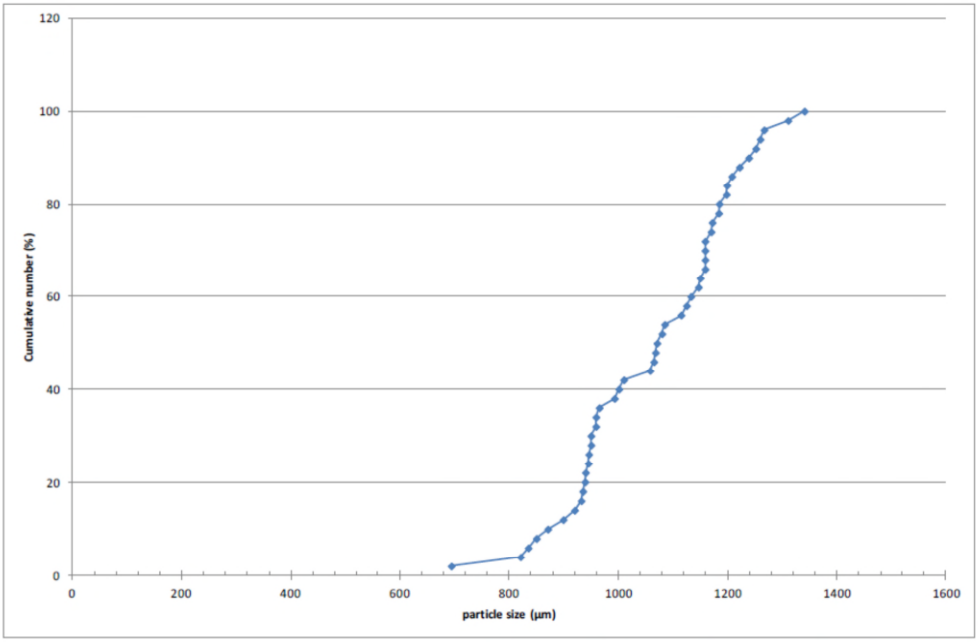


*Figure 28. Cumulative particle size distribution of the "Spannenburg 0% Bentonite" particles that have been studied for their crushing strength*

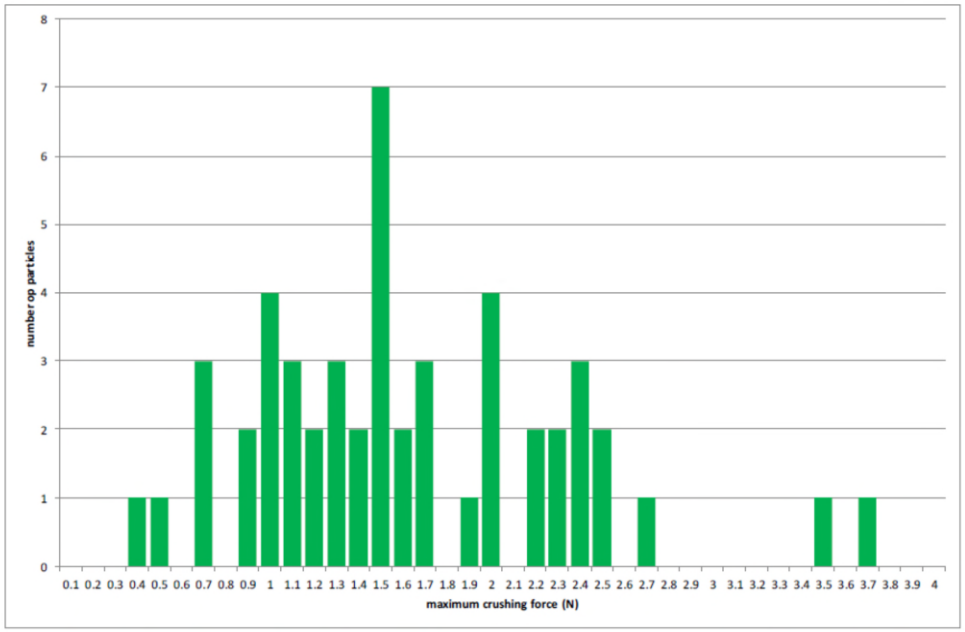


*Figure 29. Number of particles breaking at a specific crushing strength of sample "Spannenburg 1% Bentonite".*

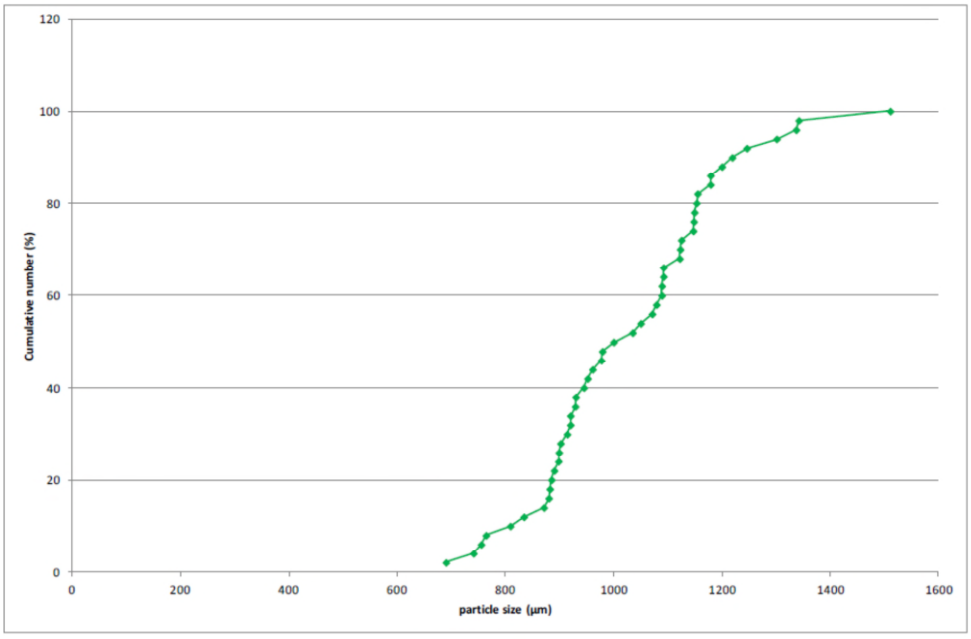


*Figure 30. Cumulative particle size distribution of the "Spannenburg 1% Bentonite" particles that have been studied for their crushing strength.*

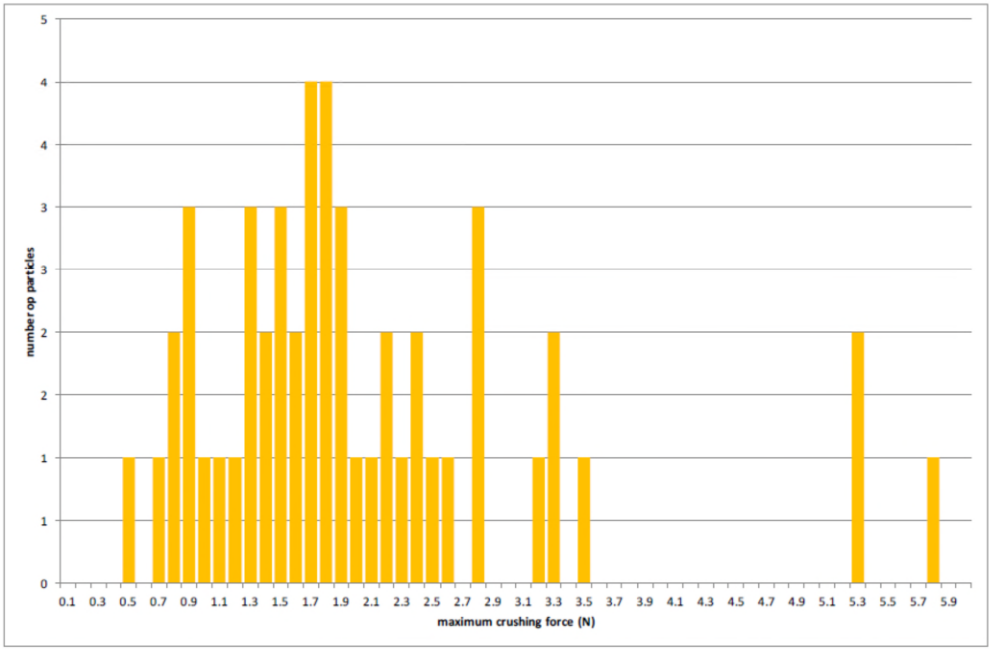


*Figure 31. Number of particles breaking at a specific crushing strength of sample "Spannenburg 2% Bentonite".*

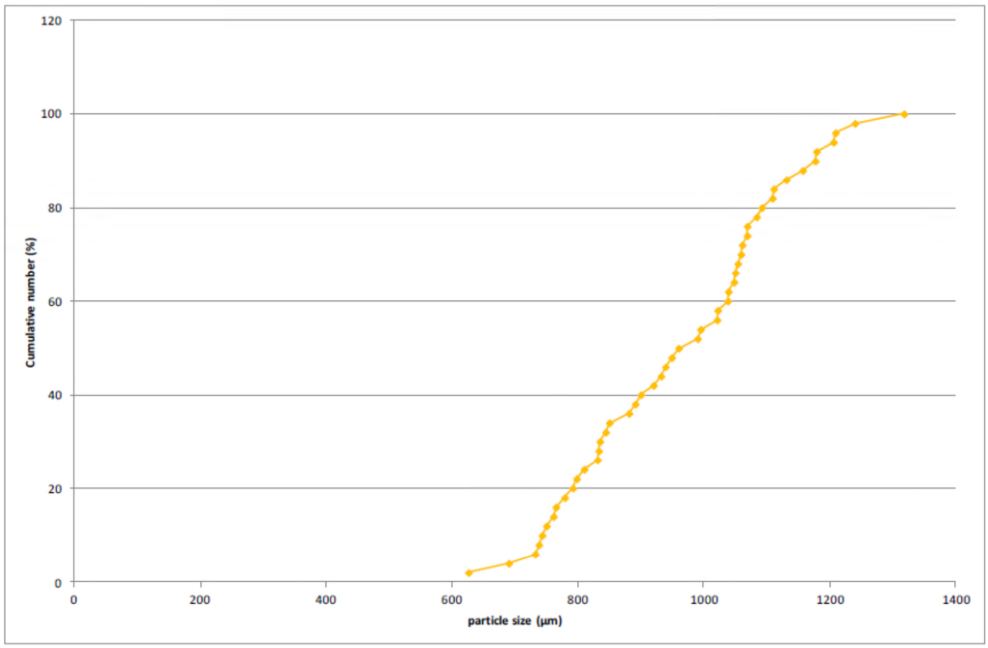


*Figure 32. Cumulative particle size distribution of the "Spannenburg 2% Bentonite" particles that have been studied for their crushing strength.*

TABLE 17. CRUSHING STRENGTH AND PARTICLE SIZE DATA OBTAINED BY APPLICATION OF THE ROBOTIC COMPRESSION TESTER OVER THE SPANNENBURG SAMPLES.

| | ***Spannenburg 0% bentonite*** | ***Spannenburg 1% bentonite*** | ***Spannenburg 2% bentonite*** |
|---|---|---|---|
| Number of measured particles | *50* | *50* | *50* |
| Average maximum force (N) | *2.7* | *1.6* | *2.0* |
| Standard deviation (N) | *1.7* | *0.7* | *1.1* |
| Average particle size (μm) | *1065* | *1027* | *962* |
| Min. Particle size (μm) | *694* | *690* | *626* |
| Median = $D_{50}$ (μm) | *1076* | *1018* | *975* |
| Maximum particle size (μm) | *1341* | *1511* | *1318* |

## References

[1] S.J. Gregg, K.S.W. Sing, "Adsorption, Surface Area and Porosity", 2nd ed., Academic Press, London, 1982.

[2] E.P. Barret, L.G. Joyner, P.H. Halenda, J. Am. Chem. Soc. 73 (1951) 373.

[3] J.C. Groen, L.A.A. Peffer, J. Pérez-Ramírez, Microporous Mesoporous Mater. 60 (2003) 1.

[4] B.C. Lippens, J.H. de Boer, J. Catal. 4 (1965) 319.

[5] J.C. Groen, J. Pérez-Ramírez and L.A.A. Peffer, in: F. Rodriguez-Reinoso, B. McEnaney, J. Rouguerol, K.K. Unger (Eds.) "Incorporation of appropriate contact angles in textural characterization by mercury porosimetry", Characterization of Porous Solids VI, Studies in Surface Science and Catalysis, Vol. 144, Elsevier, Amsterdam, 2002, pp. 91-98.

# Appendix III

## Analysis of Spannenburg material with CMC

### Crushing strength

The robotic compression tester (RCT) is an instrument for measuring the strength of particles and granules with limited supervision.

The robotic compression tester measures the maximum crushing force of individual particles or granules. The crushing force of particles with sizes ranging from 500 µm to ≈ 5000 µm can be measured. About 40 up to 100 particles are placed on a 2 cm thick smooth finely polished stainless steel plate and the coordinates of each particle and size are determined by a CCD camera. Consecutively all particles at the known coordinates are crushed and the required force is measured with a quartz force transducer. The transducer is a device that uses the piezoelectric effect to measure pressure, acceleration, strain or force by converting them to an electrical charge. The sensitive transducer is suitable for measuring quasi-static and dynamic tensile and compressive forces ranging from a few mN to 100 N.

The principal result of the compression test is an average maximum crushing force and the particle size distribution. Compressive strength of particles and agglomerates is often proportional with the particle diameter, the relationship is generally in the form: $L = k\,D^n$ where $L$ is the crushing force, $D$ is the particle diameter, $k$ and $n$ are constants depending on the material.

### Results & Discussion:

The results of the crushing strength investigations by the robotic compression tester have been summarized in Figure 33 to Figure 37 and Table 18. For sake of clarity, Figure 33, Figure 35, and Figure 37 have been plotted with the same axes in order to facilitate comparison of the three samples.

From the graphical and tabular data it becomes evident that the particles show a dissimilar crushing strength when treated at different temperatures in the range of 105˚C to 800˚C. The use of a higher temperature clearly results in a substantially and significantly higher hardness of the particles, despite the fact that the variation (standard deviation) within each sample is relatively high. The hardness increases from approx. 3.3 N for the particles heated at 105˚C, via 3.7 N at 500˚C, finally up to 10.5 N for the particles treated at 800˚C. The largest effect of temperature is thus obtained when increasing the temperature from 500˚C to 800˚C.

It furthermore appears that the use of a higher temperature (although here the effect is most prominent when comparing the samples heated at 105˚C and 500˚C) results in on average smaller particles, although the particles in the robotic compression tester have been selected randomly. A tentative explanation could be the shrinking of particles when heating them at higher temperature.

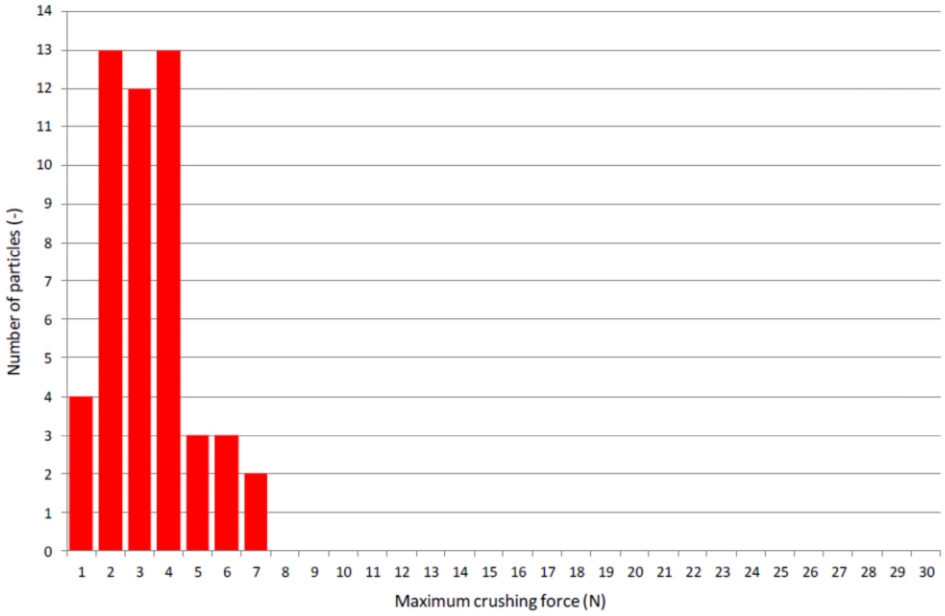


*Figure 33. Number of particles breaking at a specific crushing strength of sample "Spannenburg 105˚C".*

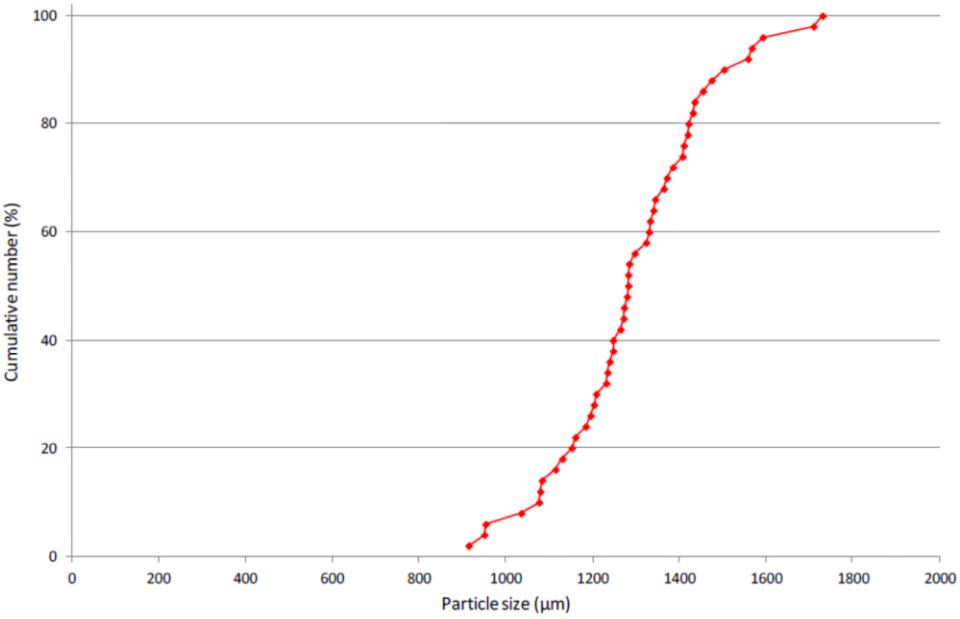


*Figure 34. Cumulative particle size distribution of the "Spannenburg 105˚C" particles that have been studied for their crushing strength.*

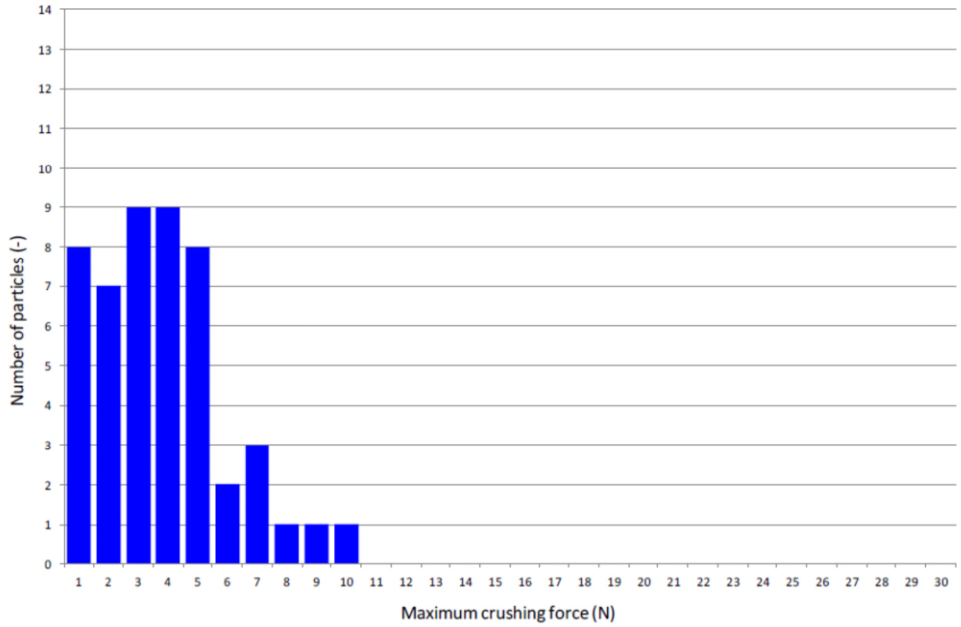


*Figure 35. Number of particles breaking at a specific crushing strength of sample "Sp-burg 500˚C".*

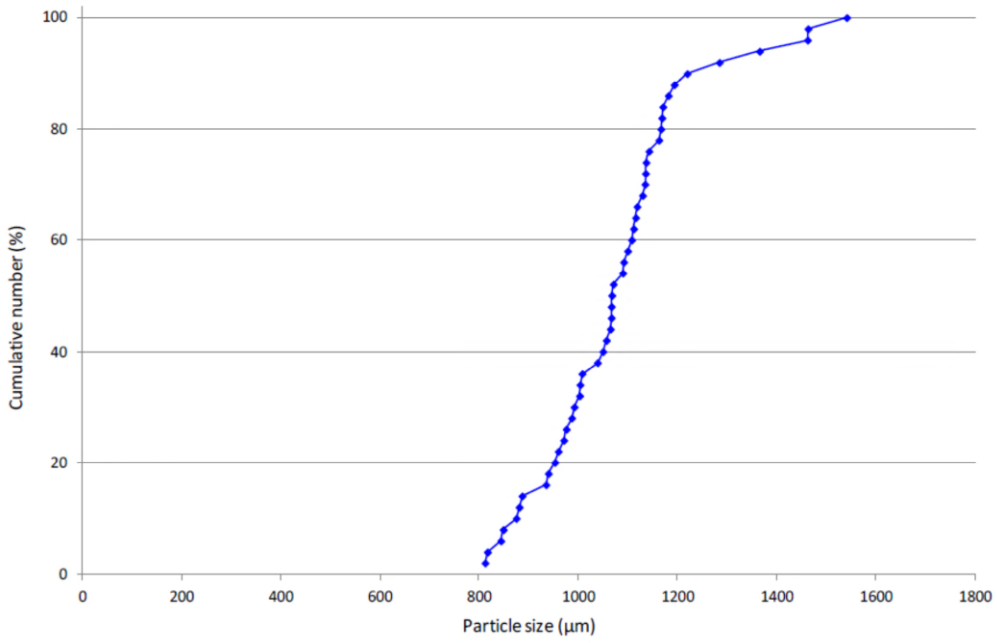


*Figure 36. Cumulative particle size distribution of the "Sp-burg 500˚C" particles that have been studied for their crushing strength.*

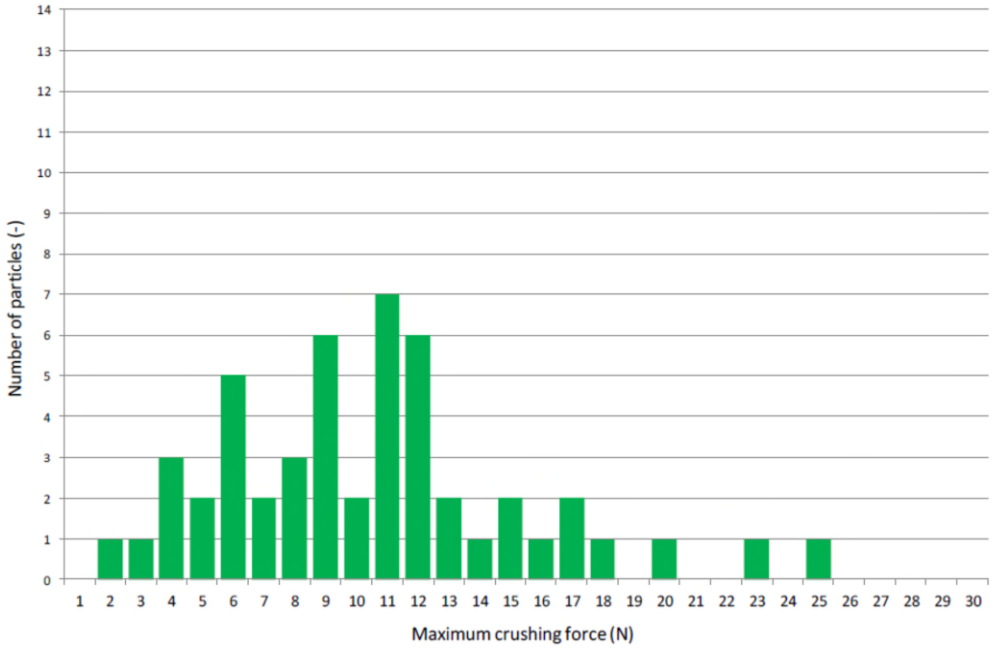


*Figure 37. Number of particles breaking at a specific crushing strength of sample "Sp-burg 800˚C".*

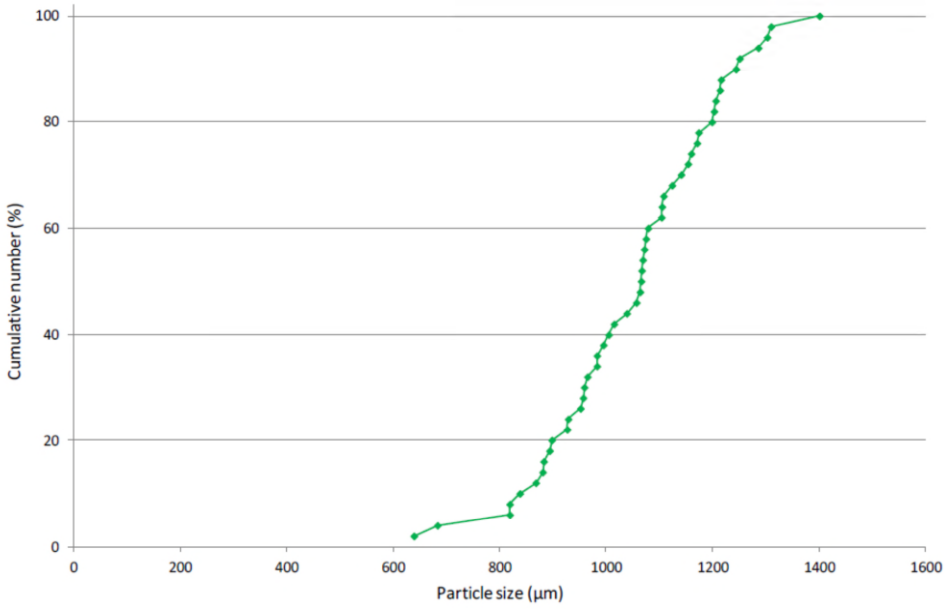


*Figure 38. Cumulative particle size distribution of the "Sp-burg 800˚C" particles that have been studied for their crushing strength.*

TABLE 18. CRUSHING STRENGTH AND PARTICLE SIZE DATA OBTAINED BY APPLICATION OF THE ROBOTIC COMPRESSION TESTER OVER THE SPANNENBURG SAMPLES.

| | Spannenburg 105 °C | Spannenburg 500 °C | Spannenburg 800 °C |
|---|---|---|---|
| Number of measured particles | 50 | 50 | 50 |
| Average maximum force (N) | 3.3 | 3.7 | 10.5 |
| Standard deviation (N) | 1.5 | 2.1 | 5.0 |
| Average particle size (µm) | 1296 | 1080 | 1051 |
| Min particle size (µm) | 915 | 812 | 639 |
| Median = D50 (µm) | 1283 | 1070 | 1066 |
| Maximum particle size (µm) | 1731 | 1542 | 1401 |

# Appendix IV

## Analyses of Spannenburg material with CMC, dried at different temperatures

### $N_2$ adsorption

Prior to the $N_2$ adsorption measurements, the samples were degassed in vacuum at 90˚C for 16 h. The dry sample weight obtained after the pre-treatment has been used in the various calculations. A part of the adsorption isotherm with $N_2$ as adsorptive was then recorded at 77 K on a Micromeritics TriStar 3000.

In $N_2$ physical gas adsorption, the sample cell holding the outgassed sample is evacuated and cooled to liquid nitrogen temperature (77 K). Portions of nitrogen are dosed into the sample cell and will be partly adsorbed on the surface, eventually getting into equilibrium with the gas phase. In this way adsorption and desorption points are recorded at different pressures and the ad- and desorption isotherm can be constructed.

Adsorbed nitrogen will first form a quasi-monolayer on the sample surface while further increase in pressure results in the formation of multilayers. In the region where monolayer and multilayers are formed, the specific surface area ($S_{BET}$) is determined according to the BET (Brunauer, Emmet and Teller) theory. This model is applicable to non-porous and meso- and macroporous materials and adsorption points in the relative pressure range between 0.05 and 0.25 are typically used (1).

### X-Ray Diffraction

The atomic and molecular structure can be attained by X-ray diffraction investigations. Crystalline atoms cause diffraction of an X-ray beam into specific directions, leading to typical reflections at certain characteristic positions in the XRD profile. In that way, the presence of crystalline matter can be identified; amorphous matter typical results in very broad, ill-defined reflections.

The X-ray powder diffraction (XRPD) patterns were recorded in a Bragg-Brentano geometry in a Bruker D5005 diffractometer equipped with Huber incident-beam monochromator and Braun PSD detector. Data collection was carried out at room temperature using monochromatic Cu radiation (Kα1 λ = 0.154056 nm) in the 2θ region between 15˚ and 95˚, step size 0.035 degrees 2θ.

The sample, of about 30 milligrams, was deposited on a Si <510> wafer and was rotated during measurement. Data evaluation was done with the Bruker program EVA. Prior to the actual analysis, the particles have been milled in order to facilitate representative sampling.

### Results & Discussion

In Figure 39 and Figure 40, the XRD patterns of the three Spannenburg samples are shown. From this comparison it becomes clear that a distinct alteration in the structural properties is obtained upon exposure to higher temperature. Whereas the sample “Spannenburg” is

mostly amorphous with one contribution from a Calcite phase, upon treatment at 500°C also contributions from a crystalline $Fe_2O_3$ phase become evident in parallel to the Calcite phase. A crystalline $Fe_2O_3$ phase becomes dominant after treatment at 800°C.

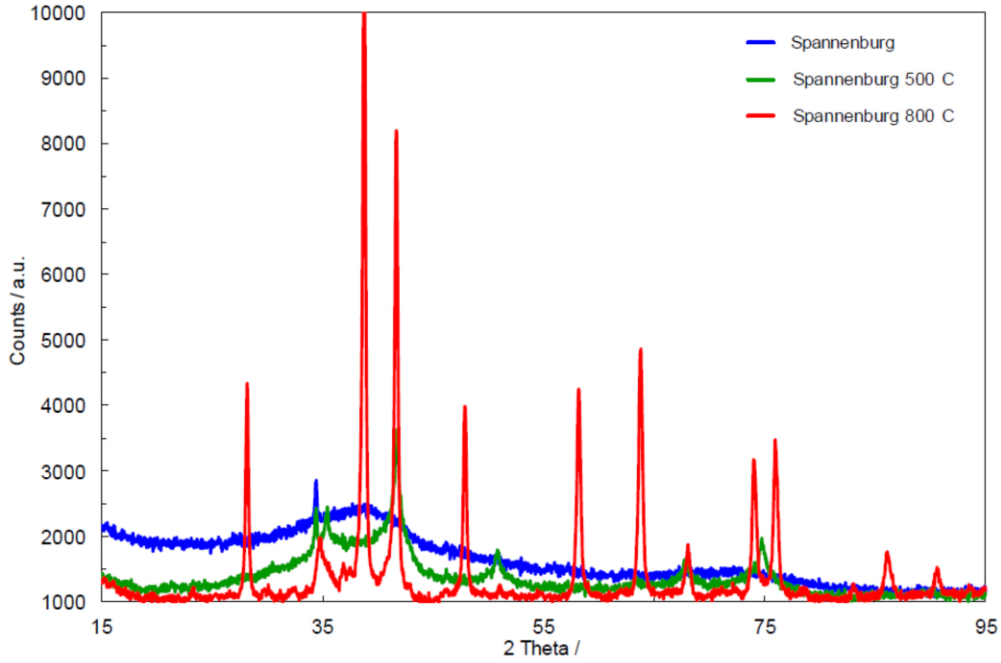


*Figure 39. XRD patterns of the three Spannenburg samples investigated.*

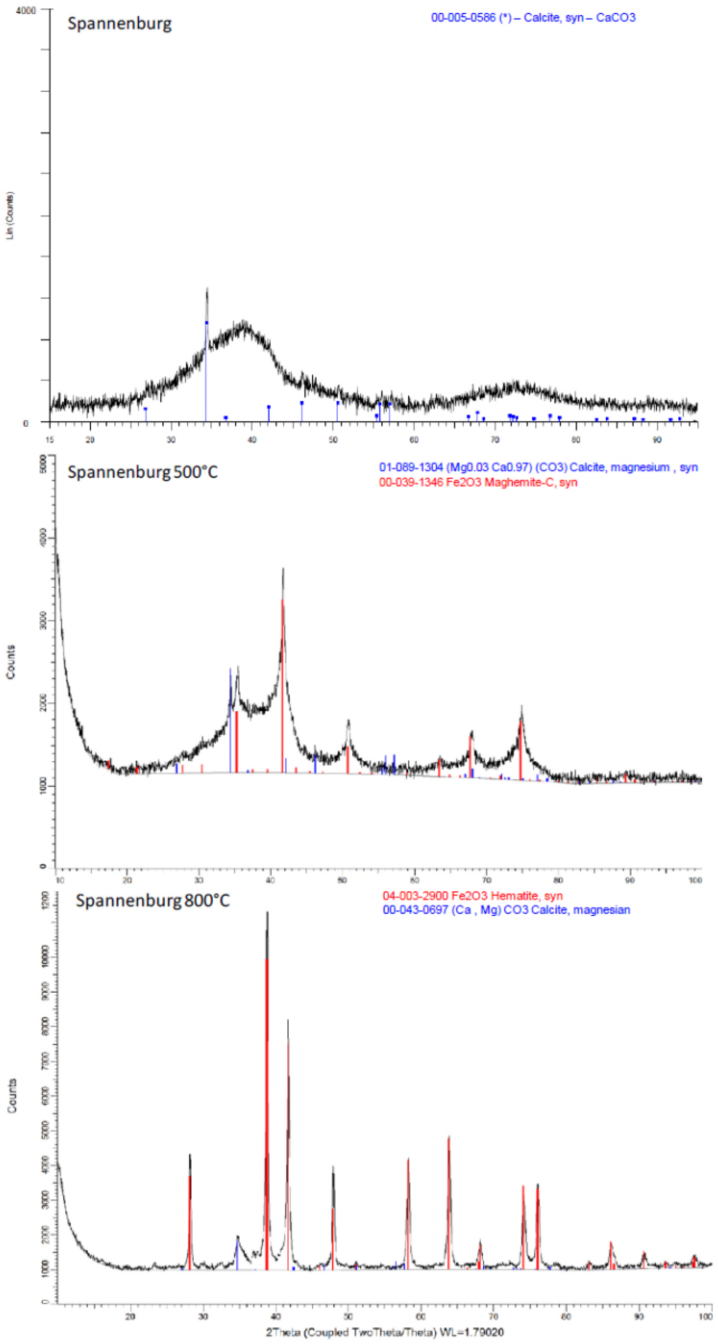


*Figure 40. Experimental and reconstructed XRD profiles of Spannenburg (top), Spannenburg 500 °C (middle) and Spannenburg 800 °C (bottom).*

It is clear from XRD that distinct structural changes occur upon treatment at higher temperature. The main question is whether the crystalline iron-containing phases developed at higher temperature positively (or negatively) impact on the adsorption capability.

In any case, it must be emphasized that the total surface area available for adsorption will also play an important role on the final adsorption properties for phosphate. To this end, the

BET surface measured by $N_2$ adsorption at 77 K has been investigated and the results are summarized in Table 19.

TABLE 19. SUMMARY OF THE BET SURFACE AREAS OF HET VARIOUS SAMPLES INVESTIGATED.

| Sample | Weight loss (wt%) | $S_{BET}$ ($m^2/g$) |
|---|---|---|
| Spannenburg | 16.8 | 230 |
| Spannenburg 500 °C | 2.5 | 54 |
| Spannenburg 800 °C | 0.1 | 8 |

Table 19 clearly demonstrates that the total surface area dramatically decreases upon treatment at higher temperature. Whereas the initial surface area is 230 $m^2 g^{-1}$, treatment of the sample at 500°C induces a tremendous decrease down to 54 $m^2 g^{-1}$, and a further decrease down to 8 $m^2 g^{-1}$ is obtained after treatment at 800°C.

Obviously, this huge loss in specific surface area should also impact on the adsorption capacity for phosphate.

*References*

[1] S.J. Gregg, K.S.W. Sing, "*Adsorption, Surface Area and Porosity*", 2nd ed., Academic Press, London, 1982.

# Appendix V

## Analysis of the Witharen sample

### N2 adsorption

Prior to the $N_2$ adsorption measurements, the sample was degassed in vacuum at 90˚C for 16 h. The dry sample weight obtained after the pre-treatment has been used in the various calculations. Then, then the adsorption and desorption isotherm with $N_2$ as adsorptive was then recorded at 77 K on a Micromeritics TriStar 3000.

In $N_2$ physical gas adsorption, the sample cell holding the outgassed sample is evacuated and cooled to liquid nitrogen temperature (77 K). Portions of nitrogen are dosed into the sample cell and will be partly adsorbed on the surface, eventually getting into equilibrium with the gas phase. In this way adsorption and desorption points are recorded at different pressures and the ad- and desorption isotherm can be constructed.

Adsorbed nitrogen will first form a quasi-monolayer on the sample surface while further increase in pressure results in the formation of multilayers. In the region where monolayer and multilayers are formed, the specific surface area ($S_{BET}$) is determined according to the BET (Brunauer, Emmet and Teller) theory. This model is applicable to non-porous and meso- and macroporous materials and adsorption points in the relative pressure range between 0.05 and 0.25 are typically used.1 In case mesopores are present in the sample under investigation, $N_2$ will condense in these pores at higher relative pressures. This information can be used to derive a mesopore size distribution, typically by means of the BJH pore size model.2-3 Besides, the empirical t-plot methodology can be used to discriminate between contributions from micropores and remaining porosity (i.e. mesoporosity, macroporosity and external surface area contributions).4

### X-Ray Diffraction

The atomic and molecular structure can be attained by X-ray diffraction investigations. Crystalline atoms cause diffraction of an X-ray beam into specific directions, leading to typical reflections at certain characteristic positions in the XRD profile. In that way, the presence of crystalline matter can be identified; amorphous matter typical results in very broad, ill-defined reflections.

The X-ray powder diffraction (XRPD) patterns were recorded in a Bragg-Brentano geometry in a Bruker D5005 diffractometer equipped with Huber incident-beam monochromator and Braun PSD detector. Data collection was carried out at room temperature using monochromatic Cu radiation (Kα1 λ = 0.154056 nm) in the 2θ region between 15˚ and 95˚, step size 0.035 degrees 2θ.

The sample, of about 30 milligrams, was deposited on a Si <510> wafer and was rotated during measurement. Data evaluation was done with the Bruker program EVA. Prior to the actual analysis, the particles have been milled in order to facilitate representative sampling.

## Results & Discussion

In Figure 41, the XRD pattern of the sample is shown. The diffraction pattern obtained clearly shows two ill-defined broad peaks resulting from a mostly amorphous phase. The only minor crystalline feature that can be resolved by pattern reconstruction can be assigned to some crystalline quartz phase, but it must be emphasized that this contribution is very low. As a consequence, it can be stated that no crystalline iron-containing phase is present in the sample and the sample must be entitled as amorphous.

Besides the structural properties, also the porous and surface area properties have been investigated. This has been realized by means of N2 adsorption at 77 K and the results are summarized in Table 20.

TABLE 20. TEXTURAL PROPERTIES OF THE SAMPLE INCLUDING THE WEIGHT LOSS OBTAINED UPON VACUUM PRE-TREATMENT

| Sample | Weight loss | $S_{BET}$ | $V_{pore}$ | $V_{micro}$ | $S_{meso}$ |
|---|---|---|---|---|---|
| | wt.% | $m^2 g^{-1}$ | $cm^3 g^{-1}$ | $cm^3 g^{-1}$ | $m^2 g^{-1}$ |
| mengsel | 2.0 | 73 | 0.162 | 0.008 | 56 |

It can be seen in Table 20 that the sample has a specific surface area of 73 $m^2 g^{-1}$. This surface area coupled to the sample weight used in the analysis (approximately 2 grams) is adequate to obtain a fully accurate analysis of the overall specific surface area. The reversibility of the desorption branch of the isotherm shown in Figure 42 also confirms the accuracy of the analysis. It can also be seen in Table 20 that the sample contains some microporosity. However, this microporosity only slightly contributes to the total specific surface area.

This is further confirmed by the isotherm, as a preferential uptake takes place at higher relative pressure. An increase in uptake at these higher relative pressures is an indication that meso- and or macropores are present in the sample. The pore size distribution of the sample, shown in Figure 43, indeed confirms the stated conclusions as mostly larger pores are present with a maximum around 20 - 30 nm.

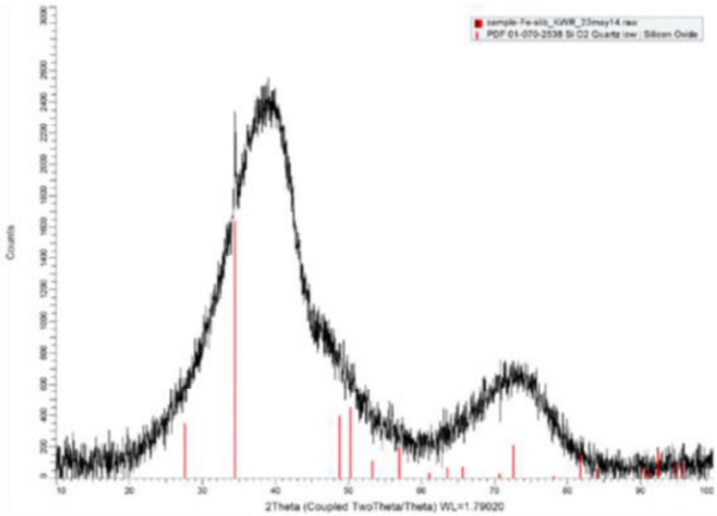


*Figure 41. XRD pattern of the sample investigated including reconstruction.*

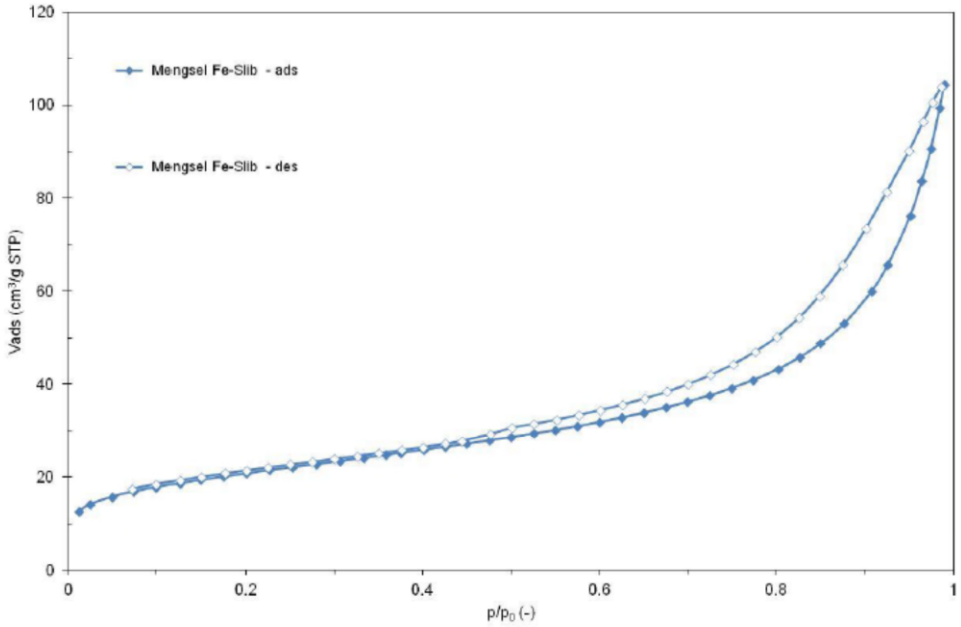


*Figure 42. $N_2$ adsorption and desorption isotherms at 77 K of the sample. Closed symbols denote adsorption, open symbols denote desorption.*

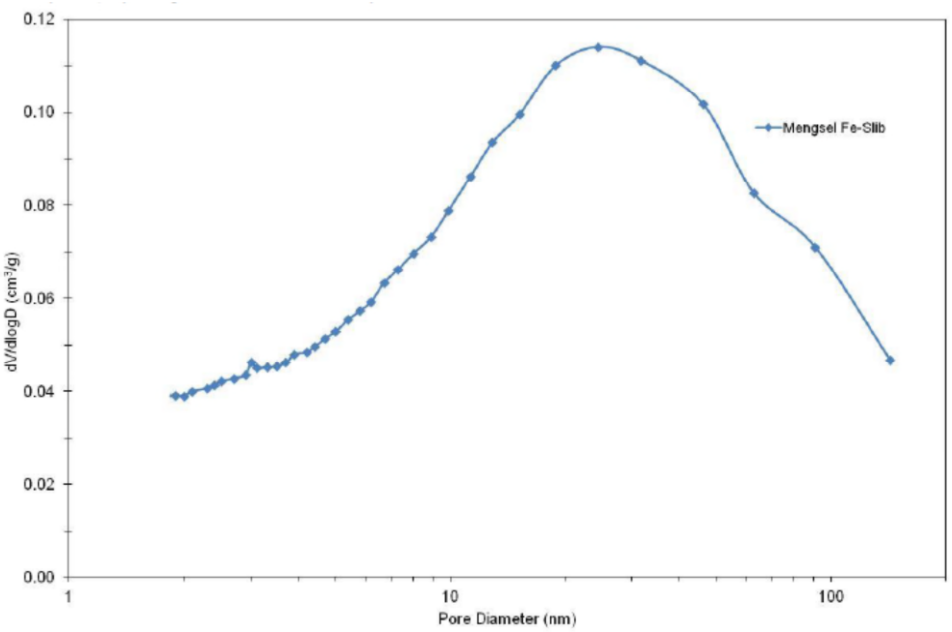


*Figure 43. BHJ pore size distribution of the sample derived from the adsorption branch of the isotherms in Figure 42.*

## References

[1] S.J. Gregg, K.S.W. Sing, "Adsorption, Surface Area and Porosity", 2nd ed., Academic Press, London, 1982.
[2] E.P. Barret, L.G. Joyner, P.H. Halenda, J. Am. Chem. Soc. 73 (1951) 373.
[3] J.C. Groen, L.A.A. Peffer, J. Pérez-Ramírez, Microporous Mesoporous Mater. 60 (2003) 1.
[4] B.C. Lippens, J.H. de Boer, J. Catal. 4 (1965) 319.

# Appendix VI

Results drying tests Ebbens Engineering

# Appendix VII

## Heavy metals, Information Ferrosorp and Lanthanum

| | Totale gehalten Arseen en zware metalen | | | | | | |
|---|---|---|---|---|---|---|---|
| | As [mg/kg] | Cd [mg/kg] | Cr [mg/kg] | Cu [mg/kg] | Ni [mg/kg] | Pb [mg/kg] | Zn [mg/kg] |
| max (FerroSorp) | 14 | 0,47 | 30 | 24 | 12 | 36 | 71 |
| FerroSorp I | 69,3 | 1,66 | 0,82 | < d.l. | 46,2 | 18,8 | 69,7 |
| FerroSorp II | 69,8 | 1,71 | 0,80 | < d.l. | 48,0 | 18,6 | 70,2 |
| | | | | | | | |
| max (Fe-slib) | 18 | 0,48 | 53 | 34 | 33 | 45 | 124 |
| Fe-slib | 5,5 ± 0,1 | 0,96 ± 0,01 | | 8,5 ± 1,3 | 7,1 ± 0,1 | 21 ± 0 | 29 ± 0 |

| | Beschikbare gehalten van As en zware metalen extractie 0,01 M CaCl2 | | | | | | |
|---|---|---|---|---|---|---|---|
| | As [mg/kg] | Cd [mg/kg] | Cr [mg/kg] | Cu [mg/kg] | Ni [mg/kg] | Pb [mg/kg] | Zn [mg/kg] |
| max | 0,9 | 0,04 | 0,63 | 0,9 | 0,44 | 2,3 | 4,5 |
| | | | | | | | |
| FerroSorp I | 0,18 | < d.l. | 0,01 | < d.l. | 0,03 | < d.l. | < d.l. |
| FerroSorp II | 0,19 | < d.l. | 0,01 | < d.l. | 0,03 | 0,01 | < d.l. |
| | | | | | | | |
| Fe-slib | 0,07 ± 0,01 | < d.l. | | < d.l. | 0,01 | 0,02 ± 0,01 | 0,01 |

| Element | Concentration of element in wt.% | |
|---|---|---|
| | Ferrosorb | Spannenburg |
| **Fe** | **49.4** | **52.6** |
| **Ca** | **6.5** | **6.2** |
| Si | 5.7 | 5.1 |
| **Mg** | **2.1** | **0.2** |
| P | 0.5 | 1.5 |
| **Mn** | **1.5** | **0.2** |
| Zr | 0.4 | 0.2 |
| Ce | 0.2 | 0.1 |
| Ba | 0.2 | 0.3 |
| Al | 0.2 | < 0.1 |
| S | < 0.1 | 0.1 |

All three Charts are based on 100% dry content and are compared to the most comparable competitor.

## Product Specification

**FerroSorp® Plus, 0,5 - 2 mm**

FerroSorp® Plus is a product with a granular structure based on Iron(III) oxide-hydroxide, FeO(OH). The use of special granulating and drying methods in the production of FerroSorp® Plus causes a high form stability and reactivity under long time aquous conditions.

| | | |
|---|---|---|
| Substance group | : | Iron(III) oxide-hydroxide |
| Formula | : | FeO(OH) |
| Ferric contents ($Fe^{3+}$) | : | minimum 40 % based on solid content |
| Ferric(III)-oxidehydrate | : | minimum 64 % based on solid content |
| Solid content | : | minimum 85 % |
| Colour | : | auburn |
| Bulk density | : | 600 ± 50 kg/m³ (loose fill), at approx. 90 % of solid content |
| | | 630 ± 50 kg/m³ (thickened fill), at approx. 90 % of solid content |
| Condition | : | granular |

**Particle size distribution**

| Particle size | | | amount | |
|---|---|---|---|---|
| < | 0,5 | mm | < 10 | % |
| | 0,5 - 0,8 | mm | 5 - 55 | % |
| | 0,8 - 1 | mm | 5 - 25 | % |
| | 1 - 2 | mm | 25 - 60 | % |
| > | 2 | mm | < 20 | % |

09/2012



**HeGo Biotec GmbH**
**Goerzallee 305b • D-14167 Berlin • Germany**
**phone: +49 (30) 847 185 50**
**fax: +49 (30) 847 185 60**
**e-Mail: info@hego-biotec.de**

## Product Specification

**FerroSorp® Plus, 2 – 4 mm**

FerroSorp® Plus is a product with a granular structure based on Iron(III) oxide-hydroxide, FeO(OH). The use of special granulating and drying methods in the production of FerroSorp® Plus causes a high form stability and reactivity under long time aquous conditions.

| | | |
|---|---|---|
| Substance group | : | Iron(III) oxide-hydroxide |
| Formula | : | FeO(OH) |
| Ferric contents ($Fe^{3+}$) | : | minimum 40 % based on solid content |
| Ferric(III)-oxidehydrate | : | minimum 64 % based on solid content |
| Solid content | : | minimum 85 % |
| Colour | : | auburn |
| Bulk density | : | 570 ± 50 kg/m³ (loose fill), at approx. 90 % of solid content |
| | | 610 ± 50 kg/m³ (thickened fill), at approx. 90 % of solid content |
| Condition | : | granular |

**Particle size distribution**

| Particle size | amount |
|---|---|
| < 2 mm | < 10 % |
| 2 - 4 mm | 70 - 95 % |
| > 4 mm | < 20 % |

09/2012



**HeGo Biotec GmbH**
**Goerzallee 305b • D-14167 Berlin • Germany**
**phone: +49 (30) 847 185 50**
**fax: +49 (30) 847 185 60**
**e-Mail: info@hego-biotec.de**

FIGUUR 33 GEMIDDELDE LANTHAANCONCENTRATIE (µg $g^{-1}$) IN WEEFSELS VAN ALLE VISSEN UIT DE COMPARTIMENTEN 1, 2, 5 EN 6 (CONTROLE) EN UIT DE PHOSLOCK® BLOOTSTELLINGEN (COMPARTIMENTEN 3 EN 4; PHOSLOCK®). ERROR BARS IS 1 SD

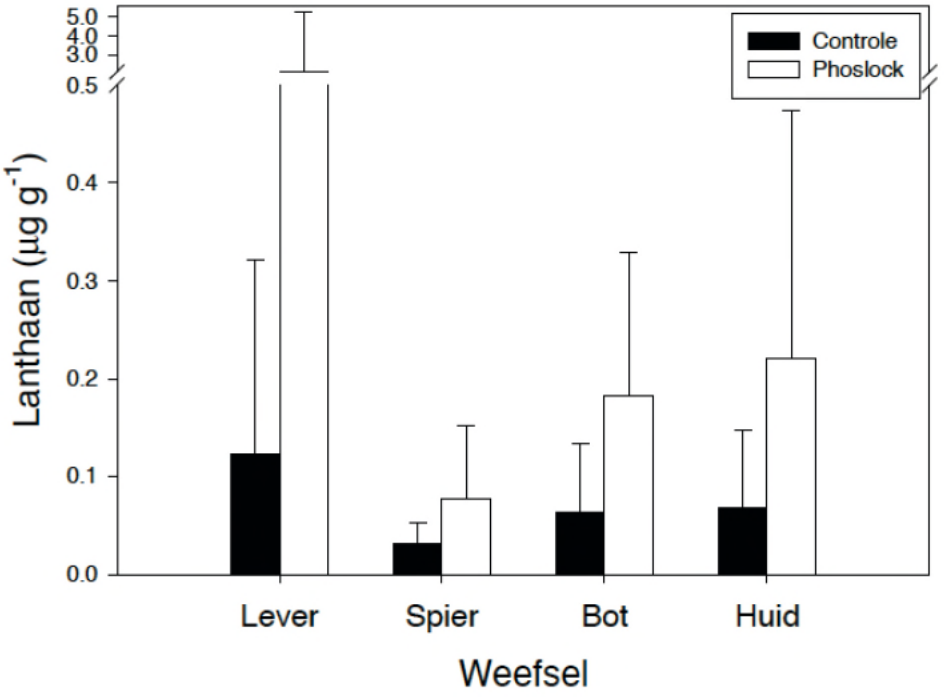


FIGUUR 54 GEMIDDELDE LANTHAANCONCENTRATIE (µg $g^{-1}$) IN WEEFSELS VAN ALLE VISSEN UIT DE COMPARTIMENTEN ZONDER EN MET PHOSLOCK® ADDITIE (COMPARTIMENTEN 3 EN 4; PHOSLOCK®). ERROR BARS GEVEN ÉÉN STANDAARDFOUT WEER

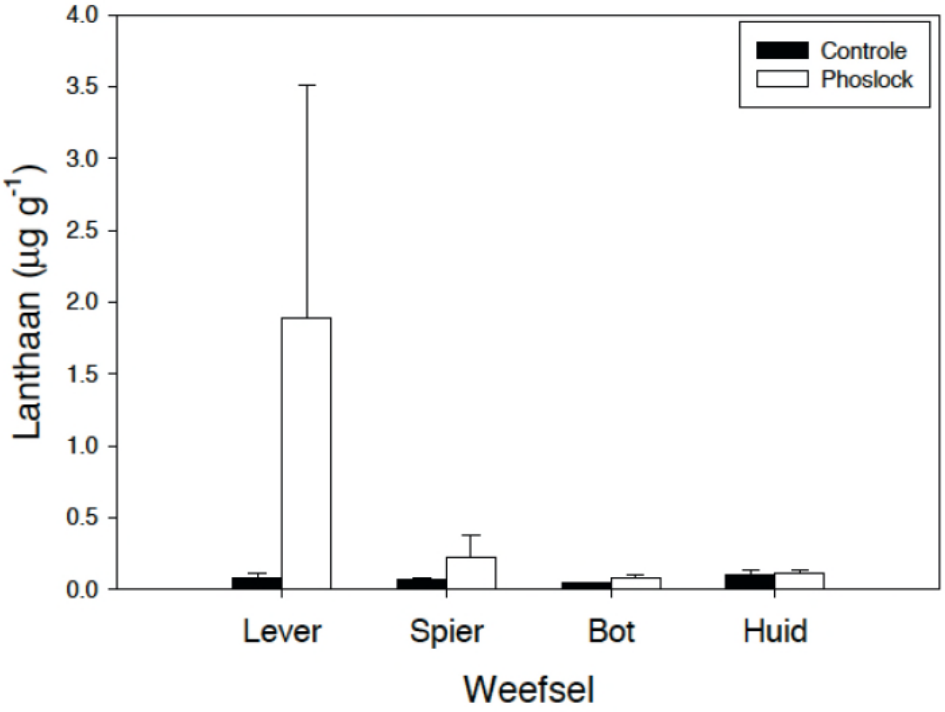

FIGUUR 69 LANTHAANCONCENTRATIES (µg $g^{-1}$) IN LEVER, BOT, SPIER EN HUID VAN AAL (A), BAARS (B), BLANKVOORN (C), BRASEM (D), SNOEK (E) EN ZEELT (F) VOOR (OPEN STAVEN) EN NA DE FLOCK & LOCK BEHANDELING (ZWARTE STAVEN). ERROR BARS GEVEN 1 SD WEER (N = 5); * GEEFT EEN SIGNIFICANT VERSCHIL (P < 0.05) AAN, NS = NIET SIGNIFICANT

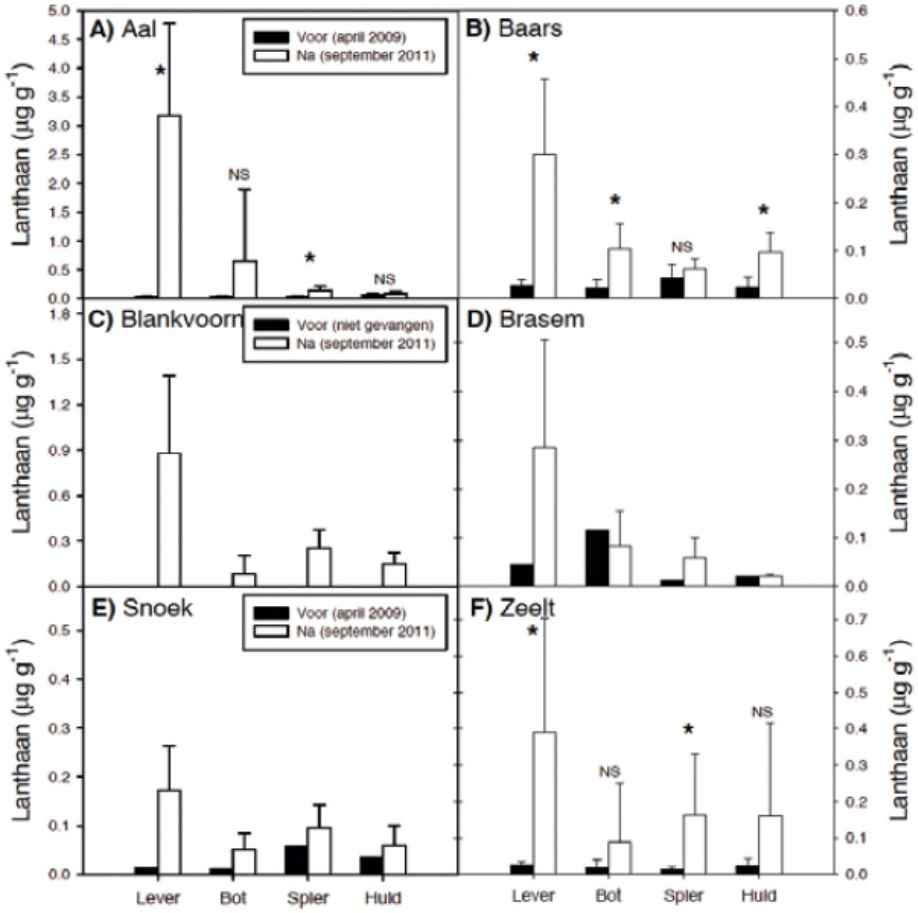


(Engels, Lurling, Turlings, & Zanten, 2012)